Integrated Multi-Disciplinary Design of a Sailplane Wing

by

Gregory J. Strauch

Thesis submitted to the Faculty of the

Virginia Polytechnic Institute and State University

in partial fulfillment of the requirements for the degree of

Master of Science

in

Aerospace and Ocean Engineering

APPROVED:

Dr. Bernard Grossman, Chairman

Dr. Raphael T. Haftka

Dr. Joseph A. Schetz

December, 1985

Blacksburg, Virginia

Integrated Multi-Disciplinary Design of a Sailplane Wing

by

Gregory J. Strauch

Dr. Bernard Grossman, Chairman

Aerospace and Ocean Engineering

(ABSTRACT)

The objective of this research is to investigate the techniques and payoffs of integrated aircraft design. Lifting line theory and beam theory are used for the analysis of the aerodynamics and the structures of a composite sailplane wing. The wing is described by 33 - 34 design variables which involve the planform geometry, the twist distribution, and thicknesses of the spar caps, spar webs, and the skin at various stations along the wing. The wing design must satisfy 30 - 31 aeroelastic, structural, aerodynamic, and performance constraints.

Two design procedures are investigated. The first, referred to as the iterative, sequential procedure, involves optimizing the aerodynamic design for maximum average cross-country speed at a constant structural weight, and then optimizing the the structural design of the resulting wing geometry for minimum weight. This value is then used in another aerodynamic optimization, and the process continues iteratively until the weight converges. The other procedure, the integrated one, simultaneously optimizes the aerodynamic and the structural design variables for either maximum average cross-country speed or minimum weight.

The integrated procedure was able to improve the value of the objective function obtained by the iterative procedure in all cases. This shows

that definite benefits can be gained from taking advantage of aerodynamic/structural interactions during the design process.

To My Parents

ACKNOWLEDGEMENTS

I am deeply indebted to Dr. Grossman and Dr. Haftka for their help and guidance in this research. I would lso like to thank all my friends in the Aerospace Department who helped me in my work and kept me sane during my extended stay at Virginia Tech. I also owe special thanks to for his guidance in the use of the Newsumt program. But I definitely owe the most gratitude to , who is now on the faculty of the ESM Department. He did all the structural/aeroelastic work involved in this project and he put up with me and my inexperience without a complaint. Without I would never have come so far as to actually write this thesis.

LIST OF SYMBOLS

A . . . . . matrix of aerodynamic influence coefficients

$A^{z\theta}$ . . . . . matrix of change in lift coefficients due to change in angles of attack

A^{zz} . . . . . matrix of change in lift coefficients due to vertical displacements

$A^{\theta\theta}$ . . . . . matrix of change in moment coefficients due to change in angles of attack

$A^{\theta z}$ . . . . . matrix of change in moment coefficients due to vertical displacements

a_e . . . . . lift-curve slope

a_{ij} . . . . . aerodynamic influence coefficient

AR . . . . . aspect ratio

c . . . . . chord length

$[\backslash c_\backslash]$ . . . . . diagonal matrix of chord lengths

C_D . . . . . drag coefficient

C_{D_i} . . . . . induced drag coefficient

C_ℓ . . . . . local lift coefficient

C_L . . . . . lift coefficient

$\{C_L^e\}$ . . . . . local lift distribution corresponding to $\{\alpha_e\}$

$\{C_L^r\}$ . . . . . local lift coefficients resulting from rigid angles of attack

$[C^{\theta\theta}]$ . . . . . matrix of torsional influence coefficients

C_{MAC} . . . . . moment coefficient about the aerodynamic center

$\{C_{MAC}\}$ . . . . . moment coefficient distribution for each wing section

D . . . . . drag force

D_i . . . . . induced drag force

$[\backslash d_\backslash]$ . . . . . diagonal matrix of the distance from the elastic axis to the center of gravity of each wing section

$[\backslash e_\backslash]$ . . . . . diagonal matrix of the distance from the elastic axis to the aerodynamic axis of each wing section

EI . . . . . modulus-weighted bending rigidity

$f(x)$ . . . . . objective function

$f(x^*)$ . . . . . local minimum of objective function

g . . . . . acceleration due to gravity

$g_q(x)$ . . . . . inequality constraints

GJ . . . . . torsional rigidity

h . . . . . vertical displacement of a wing section

H . . . . . horizontal distance covered in sailplane mission

$h_q(x)$ . . . . . equality constraints

l . . . . . local lift force

L . . . . . total lift force

N or n . . . . . load factor

NDV . . . . . number of design variables

q . . . . . dynamic pressure

q_D . . . . . dynamic pressure for divergence

s . . . . . half span of the wing

S . . . . . wing planform area

T . . . . . thrust

t . . . . . time

t/c . . . . . thickness distribution of airfoil section

U_∞ . . . . . freestream air velocity

V . . . . . velocity during cruise

V_c . . . . . climb velocity

V_R . . . . . average cross-country speed

V_s . . . . . sink speed during cruise

V_{sc} . . . . . sink speed during turn

$V_{thermal}$ . . . . . velocity of air in thermal at radius R

w . . . . . induced downwash velocity

W . . . . . total weight of loaded sailplane

$[\backslash w_\backslash]$ . . . . . diagonal weighting matrix for integration

x^i . . . . . design vector

x^* . . . . . solution design vector

y . . . . . spanwise coordinate out the wing

y_1 . . . . . general point on aerodynamic centerline where the vortex at y induces a velocity which would be induced by an infinitely long filament vortex of the same strength

LIST OF GREEK SYMBOLS

α . . . . . angle of attack

α_e . . . . . effective angle of attack

$\alpha^e(0)$ . . . . . constant obtained from the condition that the total lift introduced by the elastic deformations is zero

$\{\alpha^e\}$ . . . . . angle of attack distribution corresponding to the corrective elastic lift distribution which includes aeroelastic deformations

$\{\alpha^r\}$ . . . . . rigid twist distribution

α_{0L} . . . . . zero lift angle of attack

Γ . . . . . strength of circulation

ε . . . . . downwash angle

$\{\theta\}$ . . . . . elastic twist distribution

ρ_∞ . . . . . air density

ϕ . . . . . coordinate transformation for y in monoplane equation

TABLE OF CONTENTS

LIST OF ILLUSTRATIONS

LIST OF TABLES

1.0 INTRODUCTION

Designing an aircraft requires the integration of several disciplines in the aerospace field. The aerodynamicists design the external shape, the structural engineers design the load carrying components within, another group designs the control systems, still another group designs the engines, etc. These disciplines are usually only integrated during the preliminary design phase where simple analysis tools are used to make decisions concerning the overall shape and size parameters. After this phase in the design process, the interaction of disciplines only affects design decisions in the case of unexpected problems. For example, if the structural engineers are having problems with high stresses in the wing designed by the aerodynamics group, the two will have to work together to reach a feasible design.

This minimal interaction was sufficient for traditional airplane design because little benefit could be gained through increased interaction of disciplines due to the materials and control systems used in earlier airplanes. However, in modern airplanes, which may utilize composite materials and active controls, there is much to be gained from taking into account the interactions of disciplines in the design process. For example, with composite materials, the structure can enhance the aerodynamic performance through aeroelastic tailoring. Also, modern active control systems can have a large effect on the entire aircraft, such as preventing flutter in a wing which would normally flutter, or stabilizing

a previously unstable design. An integrated design procedure could take full advantage of these interactions throughout the design process.

Many design studies have been made which implement some of the interactions between disciplines (see references 1 - 5). In most of these studies the aerodynamic characteristics of a composite material lifting surface are improved by tailoring the ply thicknesses and orientations. This is known as aeroelastic tailoring, and a survey of its application in the U.S. is contained in Haftka[3]. In these designs, the structure was altered to enhance the aerodynamic performance. These are not truly integrated designs where both the aerodynamic and structural design of the wing are optimized at the same time to take advantage of all interactions while maximizing a performance index. However, McGeer's[5] work is more along these lines. His optimized designs involved fixing either the span loading and t/c distribution or planform and t/c distribution or span loading and planform while minimizing either induced drag or total drag. This study allowed the most interaction in the design process of the studies referenced. But it is desirable to allow even more interactions and also to take the structural weight into account in the objective function.

The objective of the present research is an investigation of the techniques and payoffs of integrated aircraft design. In order to test whether a higher level of integration results in a better design, very basic models for the aerodynamics and the structures of a simple wing were developed. These analysis methods were then used in two design procedures - one fully integrated and the other not. These models were not nearly as complete as those used in the previously mentioned designs studies,

however, these simple models could hopefully demonstrate how interactions between structures and aerodynamics could benefit an aircraft design. For example, some of the aerodynamic efficiency could be sacrificed to reduce the loads and thereby lower the structural weight and obtain better overall performance. Another possible interaction could be the use of the structural deformations incurred during flight to enhance the aerodynamic performance. If the results obtained with two basic models show the benefits of integration, then more complete models for the aerodynamics and structures, and the addition of the controls interaction, should result in still better designs.

In the spirit of keeping everything simple, the models developed were used in the design of a sailplane wing. A sailplane travels at very low speed, it has no thrust, engines, or fuel to account for, and it has a simple mission. The mission involved climbing in a thermal and then cruising to the next thermal while losing the altitude previously gained. The performance index in the mission was the average cross-country speed.

An existing sailplane with readily available, detailed design information was sought for verification of the design procedures. A sailplane designed and built at Rensselaer Polytechnic Institute (R.P.I.) was chosen to meet these requirements. The design, designated the RP-2, is sketched in Figure 1. All the required design information was acquired from references 6 - 11 and from a fact finding trip to R.P.I. .

Two design procedures were used in this study. The first was a sequential, iterative procedure and the other was an integrated procedure. The sequential, iterative procedure involved two separate programs, one for the aerodynamic design and one for the structural design. In the

aerodynamic design, the shape of the wing planform and the twist distribution were optimized for maximum cross-country speed. The calculations were done for a rigid wing at a constant weight and the optimization was subject to constraints such as no stall on the wing.

The optimized wing shape was used as input for the structural optimization program. This program minimized the weight of the composite wing by varying the spar cap and spar web areas and skin thicknesses at eight stations along the wing. This minimization was subject to constraints on maximum stress in the spar web and skin, maximum strain in the spar caps, and minimum divergence speed. This weight was used as input for another aerodynamic optimization, and the process continued until the weight converged. The final design was then used as input to another program which took the effect of wing deformations on performance into account and maximized the cross-country speed for the elastic wing.

The integrated design procedure was performed by varying the wing planform variables and the structural variables at the same time. The objective function was either the cross-country speed or total weight. This integrated approach provided more interaction between the structural design and the aerodynamic design of the wing than the separate programs used in the sequential design. And, as a result, it also provided superior designs as evidenced by the results presented in this paper.

In the next section we discuss the sailplane mission and the models and methods used for the aerodynamic and structural analysis of the designs. This is followed by a section on the design procedures and the optimization program used. Finally, the results are presented and conclusions about the benefits of integrated aircraft design are made.

2.0 MODELING OF THE SAILPLANE

2.1 PERFORMANCE

The mission chosen involved climbing to a height H in a prescribed thermal, then travelling a distance D while losing altitude H, as depicted in Figure 2. The performance index to be maximized in this mission was the average cross-country speed which is derived below. Carmichael and Horstmann thermal profiles of various strengths such as those used in Helwig[16] were considered. These profiles are shown in Figure 3.

The net rate of climb of the sailplane in the thermal is given by

$$V_c(R) = V_{thermal}(R) - V_{sc}$$

where $V_{thermal}$ is the upward velocity of the air at a distance R from the center of the thermal, and V_c is the rate of climb in the thermal. V_{sc}, the sink speed in the thermal, can be obtained in terms of C_L, C_D, the velocity, and the bank angle by assuming a small downward flight path angle. This speed is derived in Appendix A, and it is given by

$$V_{sc} = \frac{C_D}{C_L^{1.5}} \left[1 - \left(\frac{2W}{\rho S C_L g R} \right)^2 \right]^{-0.75} \left(\frac{2W}{\rho S} \right)^{0.5}$$

where W is the total weight of the plane, S is the wing planform area, g is the acceleration due to gravity, R is the radius of the turn, and C_D and C_L are the drag and lift coefficients during the turn.

The cruise speed is

$$V = (2W/\rho SC_L)^{0.5}$$

and the sink speed during cruise can be obtained in terms of C_L, C_D, and the velocity by assuming a small downward flight path angle. This speed is derived in Appendix A and is given by

$$V_s = \frac{C_D}{C_L^{1.5}} (2W/\rho S)^{0.5}$$

where C_D and C_L here are the drag and lift coefficients during cruise.

The cross country speed is determined from the mission profile as depicted in Figure 2. We define this speed as

$$V_R = D/t$$

where t is the total time of travel between points A and C, and D is the horizontal distance from A to C. The loss in height in the criuse portion of flight is given by

$$H = t_1 V_s$$

where t_1 is time of travel from A to B. The gain in height during the spiralling portion of flight is

$$H = t_2 V_c$$

where t_2 is time to travel from point B to C in Figure 2. Equating the last two equations yields

$$t_2 = t_1 \frac{V_s}{V_c}$$

And, knowing that,

$$t_1 = \frac{D}{V} \quad \text{and} \quad t = t_1 + t_2$$

results in

$$t = \frac{D}{V} (1 + V_s/V_c)$$

and, finally, the cross-country speed is found to be

$$V_R = \frac{V \cdot V_c}{V_c + V_s}$$

The cross-country speed will serve as our measure of performance in the design optimizations. Note that it is independent of the horizontal distance D and the vertical distance H.

2.2 AERODYNAMIC MODEL

2.2.1 THE MONOPLANE EQUATION

The aerodynamic loads were found using very elementary analysis techniques. The lifting forces and the induced drag were found using the monoplane equation as discussed in Bertin[19].

$$(\alpha - \alpha_{0L}) \sin \phi = \sum A_n \sin(n\phi) (\mu n + \sin \phi)$$

where $-\cos\phi = y/s$, α is the local geometric angle of attack, α_{0L} is the zero-lift angle of attack, and $\mu = ca_e/8s$ where c is the local chord length, a_e is the lift-curve slope, and s is the half span of the wing. The A_n's result from the assumption that the spanwise circulation distribution is represented by a Fourier sine series.

One of the saiplane wings was divided into 8 sections and stations were defined at the midpoint of each section as shown in Figure 4. From the geometry of the wing and the angles of attack at each station, a system of 8 equations and 8 unknowns, which were A_1 - A_8, was generated by applying the monoplane equation at each station. Once the constant A_n's were calculated, the total lift coefficient, the local lift coefficients, and the induced drag coefficient could be calculated.

This monoplane equation was obtained by assuming a spanwise circulation distribution represented by a Fourier sine series

$$\Gamma(\phi) = 4sU_\infty \sum A_n \sin(n\phi)$$

Since the spanwise lift distribution is assumed symmetrical, only the odd terms in the series remain.

The section lift force is given in Bertin[19] as

$$1(\phi) = \rho_\infty U_\infty \Gamma(\phi) = 4\rho_\infty U_\infty^2 s \sum A_n \sin(n\phi)$$

the section lift coefficient becomes

$$C_\ell(\phi) = \frac{\rho_\infty U_\infty \Gamma(\phi)}{0.5\rho_\infty U_\infty^2 c} = \frac{2\Gamma(\phi)}{U_\infty c}$$

It is also possible to find the section lift coefficient using the linear correlation between the lift and angle of attack for the equivalent two dimensional flow. Thus,

$$C_\ell = \left(\frac{\partial C_\ell}{\partial \alpha}\right)_e (\alpha_e - \alpha_{0L})$$

where α_e is the effective angle of attack.

Designating the lift curve slope as a_e and noting that $\alpha_e = \alpha - \varepsilon$, where ε is the downwash angle, yields

$$\frac{2\Gamma(\phi)}{c(\phi)a_e} = U_\infty (\alpha(\phi) - \alpha_{0L}(\phi)) - U_\infty \varepsilon(\phi)$$

Note that

$$U_\infty \varepsilon = -w = -\frac{1}{4\pi}\int_{-s}^{s} \frac{d\Gamma/dy}{y-y_1}\, dy$$

where w is the induced downwash velocity and y_1 is the general point on the aerodynamic centerline where the vortex at y induces a velocity which would be induced by an infinitely long vortex filament of the same strength.

Using the Fourier sine series for Γ and the coordinate transformation for y, one obtains

$$-w = U_\infty \frac{nA_n \sin(n\phi)}{\sin \phi}$$

This yields

$$\frac{2\Gamma}{ca_e} = U_\infty(\alpha - \alpha_{0L}) - U_\infty \frac{\sum nA_n \sin(n\phi)}{\sin \phi}$$

Using the Fourier sine series for Γ one more time results in

$$\frac{8s}{ca_e} \sum A_n \sin(n\phi) = (\alpha - \alpha_{0L}) - \frac{\sum nA_n \sin(n\phi)}{\sin \phi}$$

and defining $\mu = ca_e/8s$ gives the monoplane equation in the form shown.

2.2.1.1 Lift

The lift on the wing is defined as

$$L = \int_{-s}^{+s} \rho_\infty U_\infty \Gamma(y)\, dy = \int_0^\pi \rho_\infty U_\infty s \Gamma(\phi) \sin \phi \, d\phi$$

using the Fourier sine series for Γ,

$$L = 4\rho_\infty U_\infty^2 s^2 \int_0^\pi \sum A_n \sin(n\phi) \sin\phi \, d\phi$$

The integration yields

$$L = 4\rho_\infty U_\infty^2 s^2 \left[A_1 \left(\frac{\phi}{2} + \frac{\sin 2\phi}{4} \right)_0^\pi + \sum 0.5\, A_n \left(\frac{\sin(n-1)\phi}{n-1} - \frac{\sin(n+1)\phi}{n+1} \right)_0^\pi \right]$$

The second term on the right hand side is zero since each of the terms is zero for $n \neq 1$. So, the integral expression for lift becomes

$$L = (4s^2)(0.5\rho_\infty U_\infty^2) A_1\pi = C_L (0.5\rho_\infty U_\infty^2) \quad (5)$$

and

$$C_L = A_1\pi AR$$

where AR is the aspect ratio.

2.2.1.2 Vortex-Induced Drag

The induced drag is represented by

$$D_i = -\int_{-s}^{+s} \rho_\infty w\Gamma \, dy$$

$$= \rho_\infty \int_0^\pi \frac{U_\infty \sum nA_n \sin(n\phi)}{\sin\phi} \, 4sU_\infty \sum A_n \sin(n\phi) s \sin\phi \, d\phi$$

The integral

$$\int_0^\pi \sum nA_n \sin(n\phi) \sum A_n \sin(n\phi) \, d\phi = 0.5\pi \sum nA_n^2$$

Thus, the induced drag coefficient is

$$C_{D_i} = \pi AR \sum nA_n^2$$

2.2.2 PROFILE DRAG

The profile drag coefficients at each station were found using the local lift coefficients and the C_ℓ - C_d curve for the given airfoil section. The section used was the Boeing BoAR-80-RPVT-16B. The wing section and associated performance curves are shown in Figures 5 - 8. The profile drag coefficients were assumed to be constant over each of the sections the wing was divided into. So the total coefficient could be found by summing each local profile drag coefficient multiplied by the respective area of that section and then dividing by the total wing area.

The parasite drag coefficient of the fuselage and tails was treated as a function of the wing area as in Helwig[16] .

$$C_{D_0} = \frac{\text{constant}}{S}$$

where the constant depends on the type of aircraft.

2.2.3 VERIFICATION OF THE AERODYNAMIC MODEL

The aerodynamic analysis developed above was verified using the wing geometry of the RP-2. The computed minimum sink speed, the stall speed, and the maximum glide ratio were compared with those predicted at R.P.I., see Table 1. The differences were negligible with the only discrepancy being a 6% difference in the maximum glide ratio, but the two maximums occurred at the same airspeeds.

2.3 STRUCTURAL MODEL

2.3.1 STRUCTURAL ANALYSIS

The structural analysis was based on a simple beam model. The wing was divided into 8 constant cross section elements along the span as shown in Figure 9. Each element was an untapered two cell box beam which conformed with the shape of the airfoil at the center of each section along the span. A typical cross section is shown in Figure 10. The main spar between the two cells was an I beam with spar caps built of unidirectional graphite fibers oriented spanwise. The spar web and the skin were a sandwich construction of Kevlar face sheets with a foam core. The Kevlar fibers were oriented at ±45 degrees with respect to the spanwise direction. Because the wing had a symmetric skin layup, there was no bending-torsion coupling. All the bending loads were carried by the main spar and by assumed spanwise stringers that were obtained by lumping the axial stiffness of the total skin at five selected locations on each face of the wing. The shear flow distibution in the skin was therefore assumed to be constant between the stringers. A cross section with the stringers is shown in Figure 11.

With the wing model defined, the parameters that described the global structural behavior were the modulus-weighted bending rigidity, EI , and torsional rigidity, GJ , of each element of the wing. The torsional rigidities of each element as well as the location of the shear center of each element were obtained by carrying a shear flow analysis under the bending, twisting, and shearing loads. Once the modulus- weighted section

properties (EI and GJ) were calculated, the structural displacements were computed by numerical integration using weighting matrices and structural influence coefficients. The divergence speed was calculated using the homogeneous form of the matrix equations. Finally, the total weight of the plane was also calculated with the fuselage and tail section weight assumed to be a constant 130 kg. This was the weight of the RP-2 with a pilot minus the weight of the wings.

2.3.2 AEROELASTIC ANALYSIS

The formulation of the aeroelastic effects was based on the torsional equilibrium of a straight wing about its elastic axis considering only the effect of change in torsional deformations on the lift distribution. This involved calculating an aerodynamic matrix A where each a_{ij} is the change in lift coefficient at station j due to a unit rotation at station i. This is only the upper left matrix in the partitioned form of the full aerodynamic matrix which can be written as

$$\begin{Bmatrix} C_L \\ \hline C_{MAC} \end{Bmatrix} = \left[\begin{array}{c:c} A^{z\theta} & A^{zz} \\ \hdashline A^{\theta\theta} & A^{\theta z} \end{array}\right] \left\{\begin{array}{c} \alpha \\ \hline h \end{array}\right\}$$

Since the wing was discretized into 8 sections, the full aerodynamic matrix is a square matrix of order 16. {α} and {h} are vectors of the angle of attack and the vertical displacement of the wing at each of the 8 stations. In the present study we neglected the change in moment due to

torsional deformations and the effects due to vertical deformations. So the only matrix used from the partitioned matrix above was the $A^{z\theta}$ matrix, which will be referred to from now on as the A matrix. For a given wing geometry, the A matrix was found using the monoplane equation and unit displacement states. A base lift distribution was found for some median angle of attack at the root using the monoplane equation. Next, a unit rotation was imposed at the first station, a new lift distribution was found with the monoplane equation, and the differences between the new lift coefficients and the base lift coefficients at each of the stations formed the first column in the matrix. The other columns were found similarly to get the entire matrix.

The formulation of the static aeroelastic phenomenon follows the classical approach given in Bisplinghoff[20]. Throughout this paper, curly brackets are used for vectors, straight brackets are used for matrices, and brackets with a diagonal line inside represent diagonal matrices. The equation of equilibrium for the torsional deflections of the wing can be written as

$$\{\alpha^e\} = q[E][\backslash c_\backslash]\{C_L^e\} + \{f\} + \alpha^e(0)\{1\}$$

where $\{\alpha^e\}$ is the angle of attack distribution corresponding to the corrective elastic lift distribution due to the aeroelastic deformations, q is the dynamic pressure, $[\backslash c_\backslash]$ is the diagonal matrix of chord lengths, $\{C_L^e\}$ is the vector of local lift coefficients resulting from the elastic twist $\{\theta\}$, $\alpha^e(0)$ is the constant obtained from the condition that the total lift introduced by the elastic deformations is zero, and

$$\{f\} = q[E][\backslash c_\backslash]\{C_L^r\} + q[F]\{C_{MAC}\} - N[G]\{mg\}$$

where $\{C_L^r\}$ is the vector of local lift coefficients resulting from the rigid twist $\{\alpha^r\}$, $\{C_{MAC}\}$ is the vector of local moment coefficients found from the rigid local lift coefficients and the C_ℓ - C_m curve in Figure 8, N is the load factor, and

$$[E] = [C^{\theta\theta}][\backslash e_\backslash][\backslash w_\backslash]$$

$$[F] = [C^{\theta\theta}][\backslash c_\backslash^2][\backslash w_\backslash]$$

$$[G] = [C^{\theta\theta}][\backslash d_\backslash][\backslash w_\backslash]$$

where $[\backslash e_\backslash]$ is the diagonal matrix of the distance from the elastic axis to the aerodynamic axis for each section, $[\backslash d_\backslash]$ is the diagonal matrix of the distance from the elastic axis to the center of gravity of each wing section, $[\backslash w_\backslash]$ is the diagonal weighting matrix for numerical integration and $[C^{\theta\theta}]$ is the matrix of torsional influence coefficients, where $C^{\theta\theta}(y,\eta)$ is the twist at y due to a unit concentrated torque about the elastic axis at η.

The total lift is assumed to be constant as the wing deforms elastically, resulting in the condition that the integral of the corrective lift distribution over the span is zero. The angle of attack distribution corresponding to the corrective lift distribution is

$$\{\alpha^e\} = \alpha^e(0)\{1\} + \{\theta\}$$

$\alpha^e(0)$ expressed in matrix form is

$$\{1\}^T[\backslash w_\backslash][\backslash c_\backslash]\{C_L^e\} = 0 \quad \text{or} \quad \{1\}^T[\backslash w_\backslash][\backslash c_\backslash][A]\{\alpha^e\} = 0$$

Simultaneous solution of the equilibrium equation together with the equation above produces the elastic twist distribution, $\{\alpha^e\}$, and the constant $\alpha^e(0)$.

$$\left[\begin{array}{c|c} [\backslash 1_\backslash] - q[C^{\theta\theta}][\backslash e_\backslash][\backslash w_\backslash][\backslash c_\backslash][A] & \{-1\} \\ \hline \{1\}^T[\backslash w_\backslash][\backslash c_\backslash][A] & 0 \end{array}\right] \left\{\begin{array}{c} \{\alpha^e\} \\ \hline \alpha^e(0) \end{array}\right\} = \left\{\begin{array}{c} \{f\} \\ \hline 0 \end{array}\right\}$$

For the divergence speed calculation the homogeneous form of the equilibrium equation is used.

$$\frac{1}{q}\{\alpha^e\} = [C^{\theta\theta}][\backslash e_\backslash][\backslash w_\backslash][\backslash c_\backslash][A]\{\alpha^e\}$$

This is an eigenvalue problem, and the largest eigenvalue, $\lambda_{max} = \frac{1}{q_D}$, gives the divergence speed of the wing.

3.0 DESIGN OF THE WING

3.1 VARIABLES AND CONSTRAINTS

Our simplified design of the sailplane wing involved 33 or 34 design variables and 30 or 31 constraints, depending on the ojective function used. The design variables and the constraints are tabulated in Tables 2 and 3. The wing planform was described by variable chord lengths at the root, tip, a point in between called the break, and a variable distance to this break. The chord lengths varied linearly from root to break and from break to tip. This planform is shown in Figure 12. Geometric twist was introduced as variables at the break and the tip, with the twist varying linearly from root to break and from break to tip. The angles of attack at the root during the turning maneuver and during the cruise portion of the flight, along with the radius of the turn, are included as performance design variables. As mentioned earlier, the wing was divided into 8 sections. The spar cap thicknesses, spar web thicknesses, and the skin thicknesses were the structural design variables for each section.

The aerodynamic constraints consisted of a maximum bank angle, a minimum climb speed, no stalling of the wing at any section, and, for some cases, a performance constraint. The stall condition was simply checked by making sure that none of the local section lift coefficients exceeded the two-dimensional section stall value of 1.4 . The structural constraints were imposed at a design point for a maximum speed of 43 meters

per second and a maximum load factor of 5.9 g. This point came from the V-n diagram for the RP-2 shown in Figure 13. These constraints included stresses in the spar webs and the skin, strains in the spar caps, and a minimum divergence speed.

3.2 DESIGN PROCEDURES

Two design procedures were compared. In the first, the sequential, iterative procedure, the structural and aerodynamic optimizations were performed separately. In the second, the entire design was done in one optimization, allowing greater interaction between the structural and the aerodynamic variables in the design.

In the iterative, sequential procedure, the wing shape was first optimized for maximum cross-country speed using the planform and performance variables. This optimization was performed for a rigid wing with a given weight and was subject to the aerodynamic constraints described earlier. The optimized wing shape was then used for a separate structural program which minimized the weight of the wing by varying the structural variables while satisfying the structural constraints. This optimized weight was checked against the weight at which the aerodynamic optimization had been performed. If the two varied by more than 0.2%, then the aerodynamic optimization was performed again with the new weight. The structural weight of the resulting wing planform was minimized again, and the process continued iteratively. Once the new optimized weight and the old were within 0.2% of each other, the iteration was terminated. To correct these results for aerolastic effects, this solution was used in

another program which optimized the cross-country speed by varying only the performance variables while taking the effects of wing deformations on the performance into account. A schematic of the sequential, iterative procedure is shown in Figure 14.

The integrated design procedure combined forms of all the above programs into one. The schematic of the process is shown in Figure 15. The cross-country speed was maximized by varying all the performance, aerodynamic, and structural design variables at the same time. This allowed changes in the weight and the effects of wing deformations on the performance to be accounted for at all times during the optimization process. As a alternate way of performing the integrated design, the weight was minimized with the additional constraint of a minimum cross-country speed requirement.

3.3 OPTIMIZATION PROCEDURE

The program used for the optimization process was NEWSUMT-A. A detailed description of the program is in references 12 and 13. The basic algorithm is the sequence of unconstrained minimizations using penalty functions to account for constraints and Newton's method with approximate derivatives for unconstrained function minimizations.

Problems are formulated as follows

$$\text{Minimize} \quad f(x_1, x_2, \ldots, x_{NDV})$$

$$\text{Subject to} \quad g_q(x_1, x_2, \ldots, x_{NDV}) \geq 0 \quad q = 1,2,\ldots,n_{ineq}$$

$$\text{and} \quad h_q(x_1, x_2, \ldots, x_{NDV}) = 0$$

$$q = 1,2,\ldots,n_{eq}$$

and the side bound on the design variables

$$x_j^{(\ell)} \leq x_j \leq x_j^{(u)} \qquad j = 1,2,\ldots, NDV$$

where the functions $f(x)$, $h_q(x)$, and $g_q(x)$ are continuous and differentiable real functions with respect to the design variables x_j, $j = 1,2,\ldots, NDV$, where NDV is the number of design variables.

NEWSUMT-A systematically modifies some initial design vector while generating a sequence of vectors x^i so that $f(x)$ decreases or the degree of constraint satisfaction is improved. This sequence of vectors x converges to a solution x^* where the constraint violation is very small and $f(x^*)$ is at least a local minimum.

This program was usually found to be adequate, but, at times it did not work well when the feasible design region was very narrow. This occurred when the weight was the objective function and the performance constraint was close to the maximum possible performance. Designs which satisfied this performance constraint were in a very narrow band in the design space and NEWSUMT-A was not very efficient in that situation.

4.0 DISCUSSION OF RESULTS

We performed a series of design studies for sailplane wings in order to evaluate differences in the two design processes. The strength of the thermal was an input parameter and the results were found to be highly sensitive to this strength. Because sailplanes depend on their weight for speed during cruise, actual sailplanes often carry ballast to increase their cross-country speed. This is done when the the thermal used to climb to altitude is strong enough that the loss in climb speed due to the extra weight is outweighed by the gain in cruise speed. However, in normal airplanes minimum weight is usually desirable for maximum performance. Therefore, since the structural design process in the iterative design procedure always attempts to minimize the weight as is desired in a normal aircraft, the thermal profile chosen had to be weak enough that the sailplane weight was more critical during the climbing portion of the mission than during the cruising portion. This was done to ensure that the integrated design procedure would also minimize weight to obtain the highest cross-country speed. An extremely weak Horstmann thermal profile was chosen whose strength varied linearly from its center outward where the air moved upward at 1.22 meters per second at the center. A sketch of this profile is shown in Figure 16.

In the first series of designs, the wing span was set at 13.5 meters, which was the same as the RP-2 design. Three designs were generated. A sequential, iterative design, an integrated design maximizing cross-country speed, and a integrated design minimizing weight subject to a

minimum cross-country speed requirement equal to that obtained by the iterative design. The results and the corresponding values for the RP-2 are shown in Table 4. All these designs had better performance and lower weight than the RP-2 design, however, the RP-2 was not a fully optimized sailplane and its design was not based on the same very weak thermal profile. The increase in performance of the integrated as compared to the iterative design was only 0.95% , and the reduction in weight was 4.75%. The integrated minimum weight design had a weight 11% lower than that of the iterative design at the same cross-country performance.

Figures 17 - 20 show the angle of attack distributions for the rigid wing and the elastic wing at the 5.9 g and 43 meter per second design point for the various 13.5 meter span designs. Comparing the RP-2 design with the others indicates that 1.5 degrees of washout at the tip might be more than is needed. The other graphs indicate a trend where a larger portion of the lift is moved inboard as the weight becomes lower by introducing more downwash at the tip. This trend of moving the lift inboard is reinforced by the values of the chord lengths and the distances to the break as shown in Table 1. The chords at the break and tip decrease as the weight decreases to reduce the amount of lifting area, and therefore lifting force, on the outboard section of the wing. In addition, as the weight decreases, the wing becomes more flexible, as seen in Figure 21 which shows the torsional stiffness distributions for the various designs.

The next series of designs was made for varying wing spans with the same thermal profile used earlier. Iterated and integrated maximimized cross-country speed designs were obtained for spans of 13.5, 20, and 30 meters. An integrated design with the span as an additional design vari-

able was also obtained. These results are shown in Table 5 . The difference between the iterative and integrated designs became more apparent as the span became greater. The integrated designs had higher weights because, as the span increased, the wing area increased, and the thermal which was weak for the original designs was now strong enough for these larger area designs so that the weight was no longer critical in the climb. Minimum weight no longer meant higher cross- country speed. This trend was found by the integrated design, but the iterative design still automatically assumed that minimum weight was always the best direction to take. So, as the wing area increased and the weight was minimized for this area, the plane climbed very well in the thermal, but its cruise speed was badly depreciated because this speed decreases as wing area increases unless the weight is also increased or the lift coeficient is decreased. However, the weight was not increasing, due to the nature of the design process, and the lift coefficient could not be decreased too much or the resulting sink speed would reduce the cross-country speed. To make the iterative designs more comparable to the integrated designs for strong thermals, non-structural weight (ballast) could be added as an additional design variable.

One integrated design was obtained with the span as a design variable. This resulted in an optimal wing span of 38 meters with an aspect ratio of 60 and a weight for one wing of over 143 kilograms. These parameters combined to yield a high cross-country speed of 13 meters per second. A wing with this large a span and such a high aspect ratio may not be practical design for a marketable sailplane, but it does present a finite

limit to the benefits gained from the favorable trends found with the integrated procedure.

Another design study was performed to assess how sensitive the results were to the thermal strength. An iterated, sequential design and an integrated design for a span of 30 meters was made for very weak thermal strengths of 1.22, 0.8, 0.6, and 0.5 meters per second at the center. These results are shown in Table 6. The thermal with an 0.8 meter per second airspeed at its center was still a little too strong as indicated by the integrated design having a better performance while at a higher weight than the iterative design. The next two designs were made for a thermal with an upward airspeed of 0.6 meters per second at its center. The integrated design had a performance 9.6% higher than the iterative design and a weight 15% lower. Weakening the thermal still further to an 0.5 meter per second airspeed at its center resulted in a 7.6% increase in performance for the integrated design over the iterative, and a 10.9% decrease in weight.

We have shown that an integrated design procedure would yields designs superior to those produced by an iterative, sequential procedure using the same models for the aerodynamics and the structures. In the case of the 13.5 meter span designs, the increase in the cross-country speed between the integrated design and the iterative design was not appreciable, only 1% . But the weight minimized design with the iterative design's cross-country speed used as a constraint had a lower weight compared to the iterative design by about 11% . This reduction in weight is due to the interaction between the structural and the aerodynamic design which

resulted in a shift inboard of the lift distribution allowing a more flexible wing.

The fact that the integrated procedure yields superior designs is even more clearly illustrated by the 30 meter span designs with the two weakest thermal strengths, 0.5 and 0.6 meters per second. Because the wing was so much larger and efficient than the 13.5 meter span wing, there was much more room for improvement in the cross-country speed of the integrated designs over the iterative designs. The increase in performance of almost 10% for the integrated design over the iterative design for the stronger of the two thermals was quite appreciable. Also, this was coupled with a 15% loss in weight. The weaker thermal case shows similar results, but not quite as dramatically. This is probably because as the thermal becomes weaker, the room for improvement over the iterative design becomes less. Even so, these results are very encouraging.

The results for designs with various spans while holding the thermal strength constant indicated that the basic assumption in the iterative design procedure that minimum weight is always best was not a good assumption. This was painfully obvious, especially when the performance of the iterative designs became worse when the span increased from 20 meters to 30 meters. This was an easily recognizable mistake. But it illustrated that the integrated design process takes everything into account, while, for the iterative, sequential design process, some assumptions may have to be made and these might not necessarily be valid for all cases.

Table 7 gives a rough average of CPU time required and objective functions calculated by each design procedure. Both procedures required

about the same average amount of CPU time of around 900 seconds on an IBM 3084. This time is based on the iterative, sequential design requiring about 4 or 5 iterations. How close the initial guess for the weight was to the converged answer had a lot to do with how quickly the iterative procedure converged. In all the cases presented in this paper, the initial guess for the weight was usually within 10% of the final weight. This was because we did a very similar study earlier and the final weights of those earlier iterative designs were used as initial guesses for these latest designs to reduce cpu time. So, unless a good initial guess for the weight is available, an iterative, sequential design could easily require much more CPU time than an integrated design. Finally, the iterative, sequential designs always required more actual time than the integrated designs because each step in an iterative procedure uses information from the previous step. So there was a lot of time involved in waiting for a program to run so that the output could be used as input for the next run. However, the integrated procedure simply involved one long run that would execute overnight.

5.0 CONCLUSIONS

Our investigation of the design process of a composite sailplane wing clearly demonstrates the superiority of an integrated design approach over an iterative, sequential procedure. Within the assumptions of very rudimentary aerodynamic and structural analyses, the integrated optimization procedure yielded superior designs. These designs resulted because the optimizer was able to find favorable trends in the design space which resulted from interactions between the aerodynamics and the structures. These interactions included distributing the structural material so the deformations did not reduce the aerodynamic performance, and reducing the weight of the wing to increase the overall performance. Wing weight was reduced by concentrating more of the lift on the inboard portion of the wing and by reducing the planform area of the wing. Shifting the weight inboard resulted in lower root bending moments, thus allowing less structural material at the root without violating the stress constraints. Decreasing the planform area was accomplished by reducing the chord lengths out the wing since the span was held constant. The shorter chord lengths resulted in less torsional stiffness which led to greater deformations. But this did not depreciate the aerodynamic performance because the added deformations were taken into account by adding twist and distributing the structural material prudently. The separation of the two disciplines in the iterative procedure did not allow such interactions to be taken into account and applied towards improvement of the design.

The next step in the formulation of a complete integrated design process is to allow a more arbitrary wing shape and to use more exact methods for analyzing the aeodynamics and the structures. An arbitrary wing would include chord length and twist variations at each station, and the addition of the thickness distribution of the airfoil section profile at each station as a design variable. A more exact aerodynamic analysis would entail using something better than lifting line theory, such as vortex panel methods, to obtain the lift distribution and the induced drag. then some form of boundary layer analysis would have to be added to account for the skin friction drag and the form drag. The next step in the structural analysis is to go to a finite element method allowing more freedom and higher accuracy in the structural design.

To utilize the more complex analysis techniques described above, many geometric points will have to be added as design variables. As the number of design variables increases, so does the number of constraints. Completing an optimized design with such a huge amount of design variables and constraints for a vehicle more complex than a sailplane, such as a transport, would even stretch the limits of today's supercomputers. And this is just for the wing. If the whole plane and all its systems were included, the time required for a complete optimization would become completely impractical with existing computers. But this study shows that the benefits of an integrated multi-disciplinary design process make working towards a useful design procedure in the future very worthwhile.

LIST OF REFERENCES

1. Ashley, H., "On Making Things the Best - Aeronautical Uses of Optimization", AIAA Aircraft Systems and Technology Conference , Dayton, Ohio, August 1981.

2. Austin, F., et al, "Aeroelastic Tailoring of Advanced Composite Lifting Surfaces in Preliminary Design", Proceedings AIAA/ASME/SAE 17th Structural Conference , King of Prussia, Penn., May 1976.

3. Haftka, R.T., Structural Shape Optimization with Aeroelastic Constraints - A Survey of US Applications , Virginia Polytechnic Institute and State University

4. Lynch, R.W. and W.A. Rogers, "Aeroelastic Tailoring of Composite Materials to Improve Performance" ,Proceedings AIAA/ASME/SAE Structural Conference, King of Prussia, Penn., May 1976.

5. McGeer, Tad, Wing Design for Minimum Drag and Practical Constraints , Phd. Stanford University, 1984.

6. Bundy, Francis P. and N.Y. Alplaus, "Composite Materials, Engineering and Gliders at RPI" ,Hangar Flying, 1983-84.

7. Helwig, H.G., "Capglide and the RP-1" ,Soaring, February 1980, pp.22-25

8. Winkler, S.J., Aeroelastic Analysis of a Composite Wing , M.S., Rensselaer Polytechnic Institute, 1981.

9. Winkler, S.J. and Francis P. Bundy, Progress Report on RPI's RP-2 Glider ,RPI, Troy, New York, 1982.

10. Winckler, S.J. and Francis P. Bundy, "Rensselaer's 'Homebuilt' RP-2" ,Soaring, June 1983, pp. 26-29

11. Winkler, S.J., "RPI's Capglide Program" ,AIAA Student Journal, Spring 1981, pp. 44-48

12. Miura, Hirokazu and Lucien A. Schmit, Jr., NEWSUMT - A Fortran Program for Inequality Constrained Function Minimization - Users Guide , University of California, Los Angeles

13. Thareja, Rajiv and R.T. Haftka, NEWSUMT - A A Modified Version of NEWSUMT for Inequality and Equality Constraints , Virginia Polytechnic Institute and State University, March 1985.

14. Boermans, L.M.M., "Development of Computer Program for Parametric Sailplane Performance Optimization" ,Aero-Revue, May 1983, pp.280-285

15. Eppler, Richard, "The Optimum Design and Wing Section of a 15 Meter Glider Without Flaps" ,Sailplane and Gliding, July 1977, pp. 110-117

16. Helwig, Gunter, Wing Shape Optimization for Maximum Cross-Country Speed with Mathematical Programming , Renssalaer Polytechnic Institute, N79-23899, 1979.

17. Irving, F.G., Computer Analysis of the Performance of 15 Meter Sailplanes , Imperial College of Science and Technology, London, England Nov. 1973

18. Abbot, Ira H. and Albert E. Von Doenhoff, Theory of Wing Sections , Dover Publications Inc., N.Y. 1954.

19. Bertin, John J. and Michael L. Smith, Aerodynamics for Engineers , Prentice Hall Inc., Englewood Cliffs, N.J. 1979.

20. Bisplinghoff, R.L., H. Ashley, and R.L. Hoffman, Aeroelasticity , Addison-Wesley Publishing Co., Reading, Mass. 1955.

21. Eppler, R., A Computer Program for the Design and Analysis of Low Speed Airfoils , NASA TM-80210, August 1980.

22. Fiacco, A.V. and G.P. McCormick, Nonlinear Programming: Sequential Unconstrained Minimization Techniques , John Wiley and Sons Inc. 1968.

23. Grossman, B., Integrated Multidisciplinary Design - Semi Annual Report , VPI&SU 1985.

24. Grossman, B., Integrated Multidisciplinary Aircraft Design , VPI&SU 1985.

25. Gurdal, Zafer, Integrated Aerodynamic/Structural Wing Design for a Lightweight Glider , VPI&SU 1985

26. Haftka, R.T., "Optimization of Flexible Wing Structures Subject to Strength and Induced Drag Constraints" ,AIAA Journal, Volume 14, 1977, pp.1101-1106

27. Haftka, R.T. and J.H. Starnes, "Application of a Quadratic Extended Interior Penalty Function for Structural Optimization" ,AIAA Journal, Volume 14, June 1976, pp.718-724

28. Haftka, R.T. and Ramana V. Grandhi, "Structural Shape Optimization - A Survey" ,AIAA/ASME/ASCE/AHS 26th Structures, Structural Dynamics and Materials Conference

29. Jones, R.T., "The Spanwise Distribution of Lift for Minimum Induced Drag of Wings Having a Given Lift and Root Bending Moment", NACA TN 2249, Dec. 1950.

30. Klein, A. and S.P. Viswanathan, "Approximate Solution for Minimum Induced Drag of Wings with Given Structural Weight" ,Journal of Aircraft, Volume 12, Feb. 1975, pp.124-126

31. Krane, Norris J. Jr., "Divergence Elimination with Advanced Composites" , AIAA Journal, 1975.

32. Lobert, G., "Spanwise Lift Distribution of Forward and Aft Swept Wings in Comparison with Optimum Distribution Form" , Journal of Aircraft, Volume 18, June 1981, pp.496-498

33. Munk, Max, "The Minimum Induced Drag of Aerofoils" , Classical Aerodynamic Theory, N80-15038, Dec. 1979.

34. Muser, Dieter, Advanced Composites in Sailplane Structures: Applications and Mechanical Properties, N79-27079, 1979.

35. Perkins, Courtland D., and Robert E. Hage , Airplane Performance Stability and Control, John Wiley and Sons, Inc., New York, 1949.

Table 1.

Characteristics Data for RP-2 Glider

OVERALL:		
Span	13.5 m	44.25 ft
Length	6.6 m	21.65 ft
Height	1.25 m	4.1 ft
WING:		
Area	11.1 sq. m	120 sq. ft
Aspect Ratio	16.4	
Section	BOAF-163	
VERTICAL STABILIZER:		
Span	1.25 m	4.1 ft
Area	0.5 sq. m	5.4 sq. ft
Section Profile	FX-L-III-142	
HORIZONTAL STABILIZER:		
Span	2.5 m	8.2 ft
Area	1.0 sq. m	10.8 sq. ft
Section Profile	FX-L-III-142	
PERFOR ANCE AT GROSS WEIGHT OF 160 kg(353 lbs):		
Stall speed w/o flaps	47 km/hr	29 mph
Min. sink rate	0.53 m/sec	1.7 fps
Max. glide ratio	28 at 61 km/hr	
EMPTY WEIGHT (esimated):	78 kg	172 lbs

Table 2.

Design Variables

3 Performance Design Variables	1. Angle of attack at the root during the turn
	2. Angle of attack at the root during cruise
	3. Radius of the turn
6 Geometric Design Variables	4. Angle of twist at the break relative to the root
	5. Angle of twist at the tip relative to the root
	6. Chord length at the root
	7. Chord length at the break
	8. Chord length at the tip
	9. Distance to the break
24 Structural Design Variables	10 - 17. Spar cap thickness for each wing section
	18 - 25. Spar web thickness for each wing section
	26 - 33. Skin thickness for each wing section

Semi-span was also used as a design variable for one design.

Table 3.

Design Constraints

3 Stall Constraints during turning maneuver	1. No stall at the root
	2. No stall at the break
	3. No stall at the tip
3 Performance Constraints	4. Bank angle less than 50°
	5. Climb speed greater than zero
	6. Minimum divergence speed
24 Structural Constraints	7 - 14. Maximum spar cap strain for each wing section
	15 - 22. Maximum shear stress for each wing section
	23 - 30. Wing skin must satisfy Tsai-Hill strength constraint for each wing section

Minimum average cross-country speed was also used as a constraint for weight minimized designs.

Table 4.

13.5 Meter Span Results

	ITERATED SEQUENTIAL	INTEGRATED DESIGN	WEIGHT MINIMIZATION	RP-2 BASELINE
CROSS-COUNTRY SPEED (M/S)	7.40	7.47	7.40	7.22
MASS OF ONE WING (KG)	12.6	12.0	11.2	14.2
CHORD LENGTH				
ROOT	99	97	97	95
BREAK (CM)	99	94	89	95
TIP	34	31	27	50
DISTANCE TO BREAK (CM)	312	298	282	300
TWIST (DEGREES)				
BREAK	0.16	0.05	0.24	0.0
TIP	0.06	-0.42	-0.62	-1.5
ASPECT RATIO	16.3	17.1	18.1	16.2
WING AREA (M^2)	11.2	10.7	10.1	11.2

Table 5.

Effects of Varying the Span

	SPAN (M)	CROSS-COUNTRY SPEED (M/S)	MASS OF ONE WING (KG)	ASPECT RATIO	WING AREA (M**2)
SEQUENTIAL	13.5	7.40	12.6	16.3	11.2
INTEGRATED	13.5	7.47	12.0	17.1	10.7
SEQUENTIAL	20.0	10.07	18.5	27.4	14.6
INTEGRATED	20.0	10.26	21.5	28.5	14.0
SEQUENTIAL	30.0	7.60	38.9	49.3	18.3
INTEGRATED	30.0	11.83	110.0	40.3	22.3
SPAN FREE DESIGN	38.0	12.97	143.7	60.3	23.9

Table 6.

Thermal Strength Effects

for 30 Meter Span

	THERMAL STRENGTH (M/S)	CROSS-COUNTRY SPEED (M/S)	MASS OF ONE WING (KG)	ASPECT RATIO	WING AREA (M**2)
SEQUENTIAL	1.22	7.60	38.9	49.3	18.3
INTEGRATED	1.22	11.83	110.0	40.3	22.3
SEQUENTIAL	0.80	8.12	42.1	42.4	21.2
INTEGRATED	0.80	8.25	44.2	43.5	20.7
SEQUENTIAL	0.60	5.09	46.9	37.2	24.2
INTEGRATED	0.60	5.58	39.8	40.0	22.5
SEQUENTIAL	0.50	3.22	44.9	35.7	25.2
INTEGRATED	0.50	3.46	40.0	37.0	24.3

Table 7.

Average Final Statistics

INTEGRATED DESIGN

3100	OBJECTIVE FUNCTIONS
33	DESIGN VARIABLES
900	SECONDS CPU TIME - IBM 3084

ITERATED SEQUENTIAL DESIGN

AERODYNAMIC (PER ITERATION)

700	OBJECTIVE FUNCTIONS
9	DESIGN VARIABLES
80	SECONDS CPU TIME - IBM 3084

STRUCTURAL (PER ITERATION)

2000	OBJECTIVE FUNCTIONS
24	DESIGN VARIABLES
120	SECONDS CPU TIME - IBM 3084

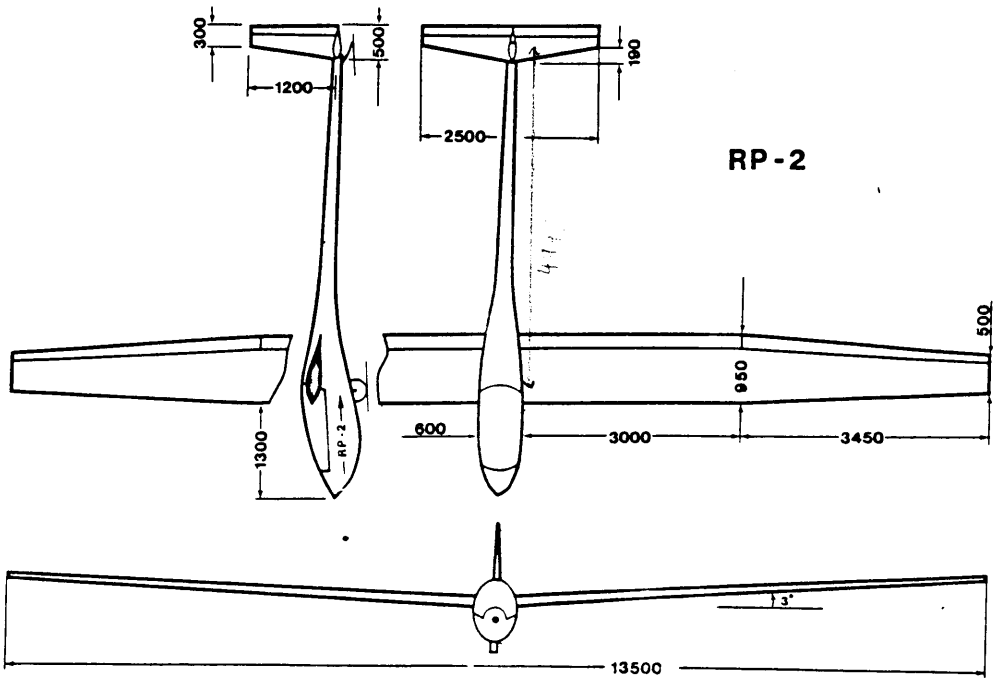

Figure 1. RP-2 Glider

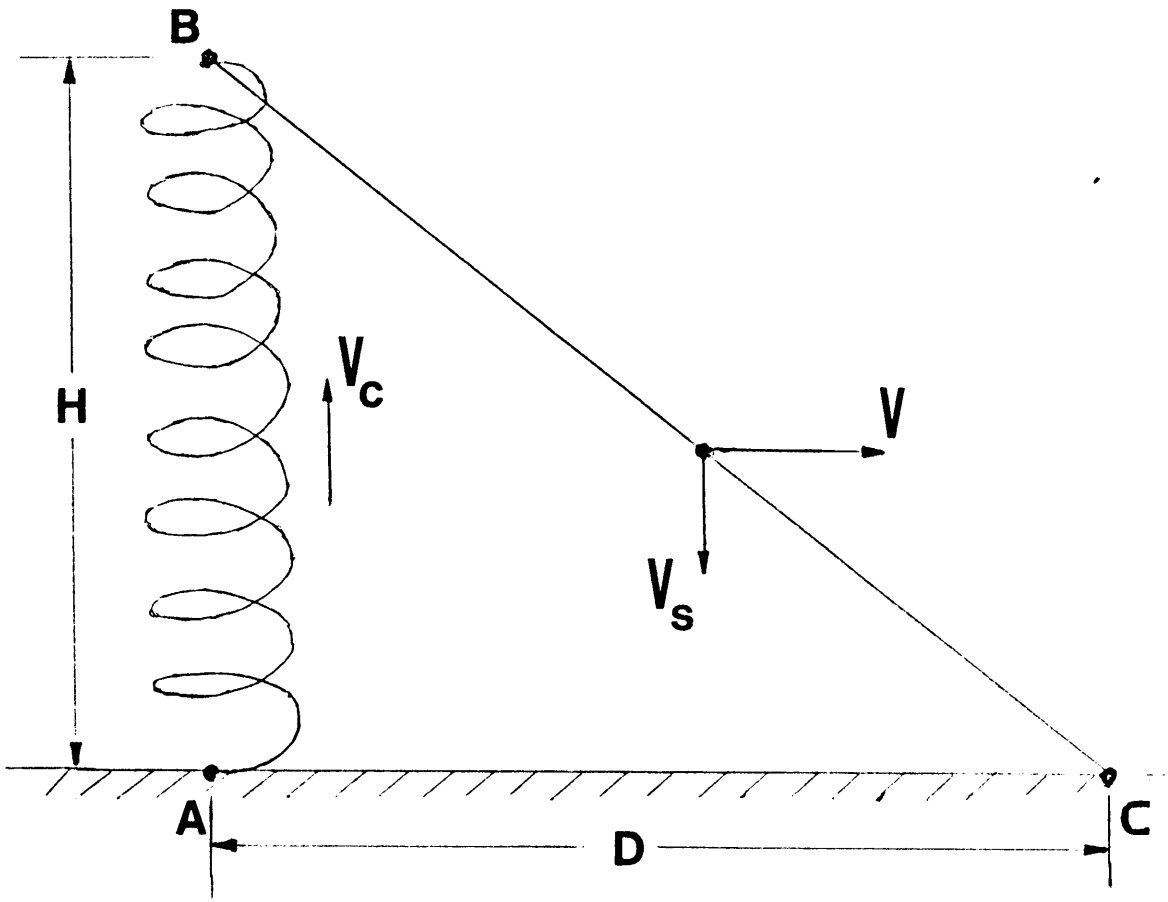

Figure 2. Sailplane Mission Profile

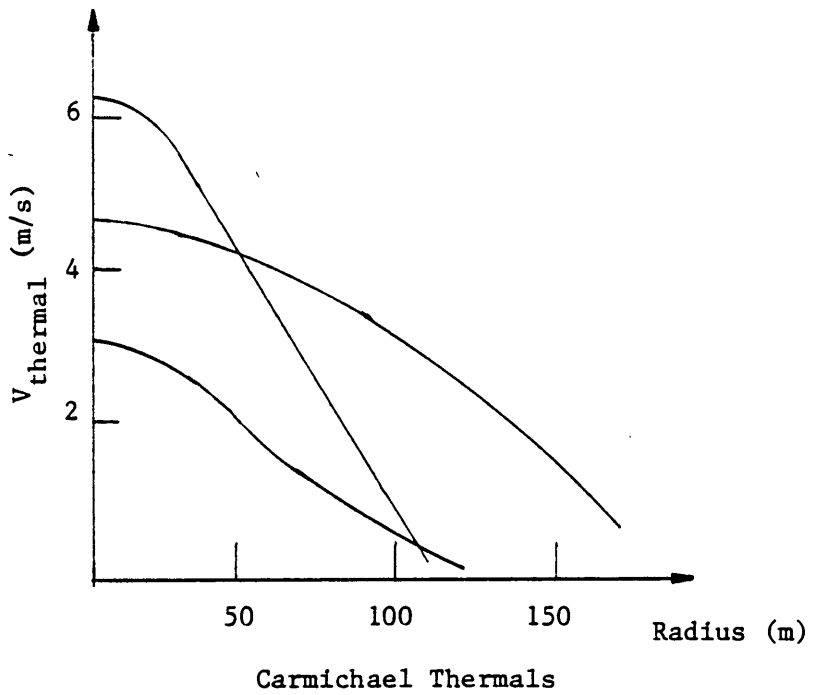

Carmichael Thermals

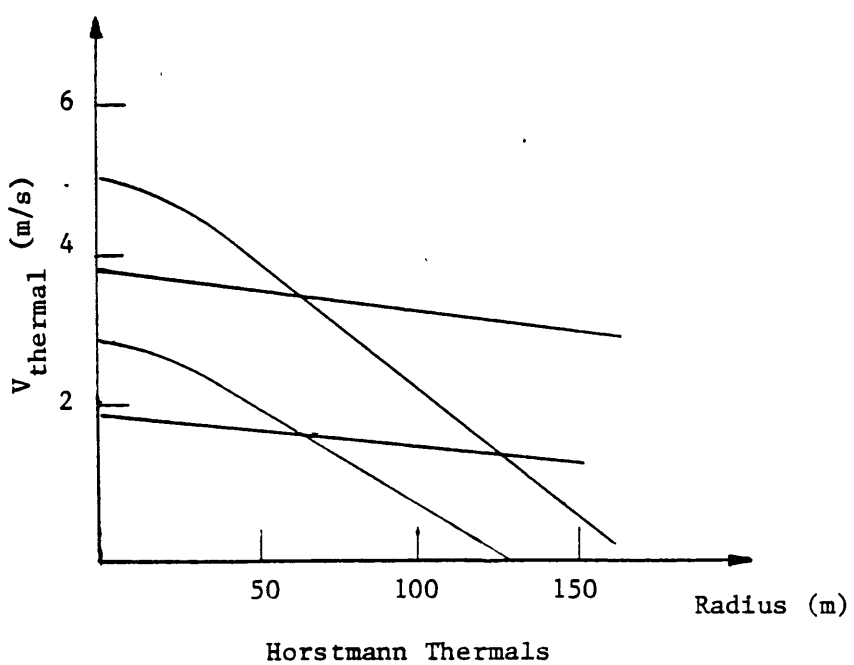

Horstmann Thermals

Figure 3. Thermal Profiles

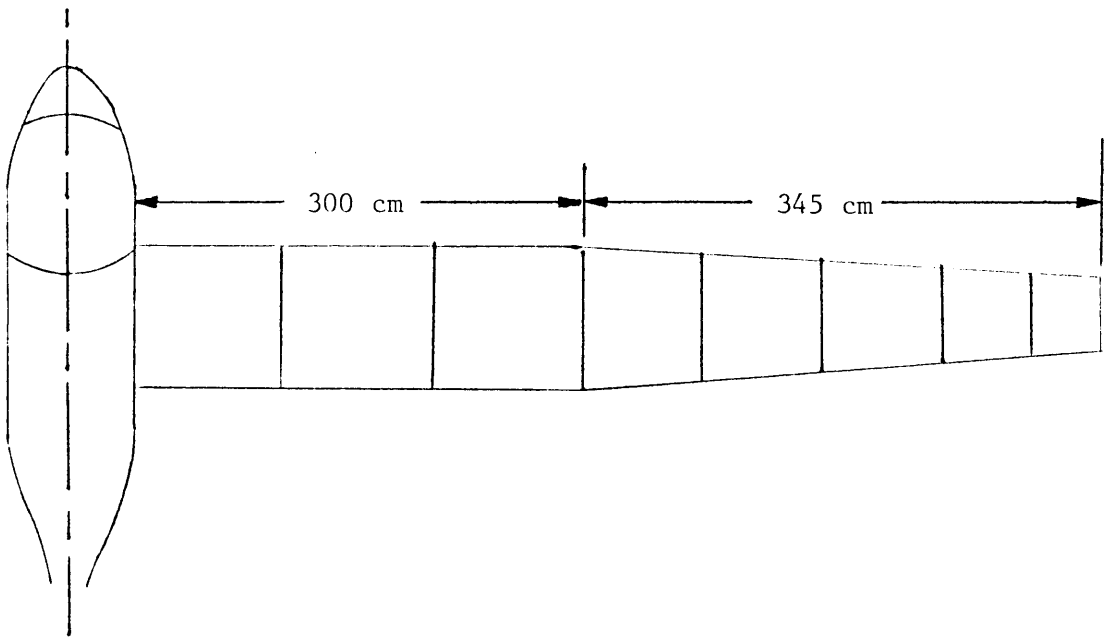

Figure 4. RP-2 Wing Divided in Sections

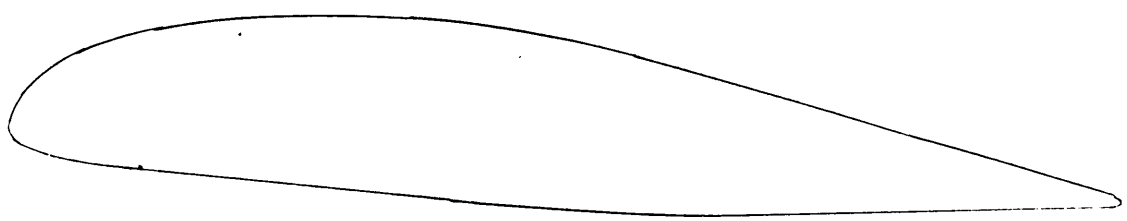

Figure 5. BoAR 80-RPVT-163 Airfoil Section

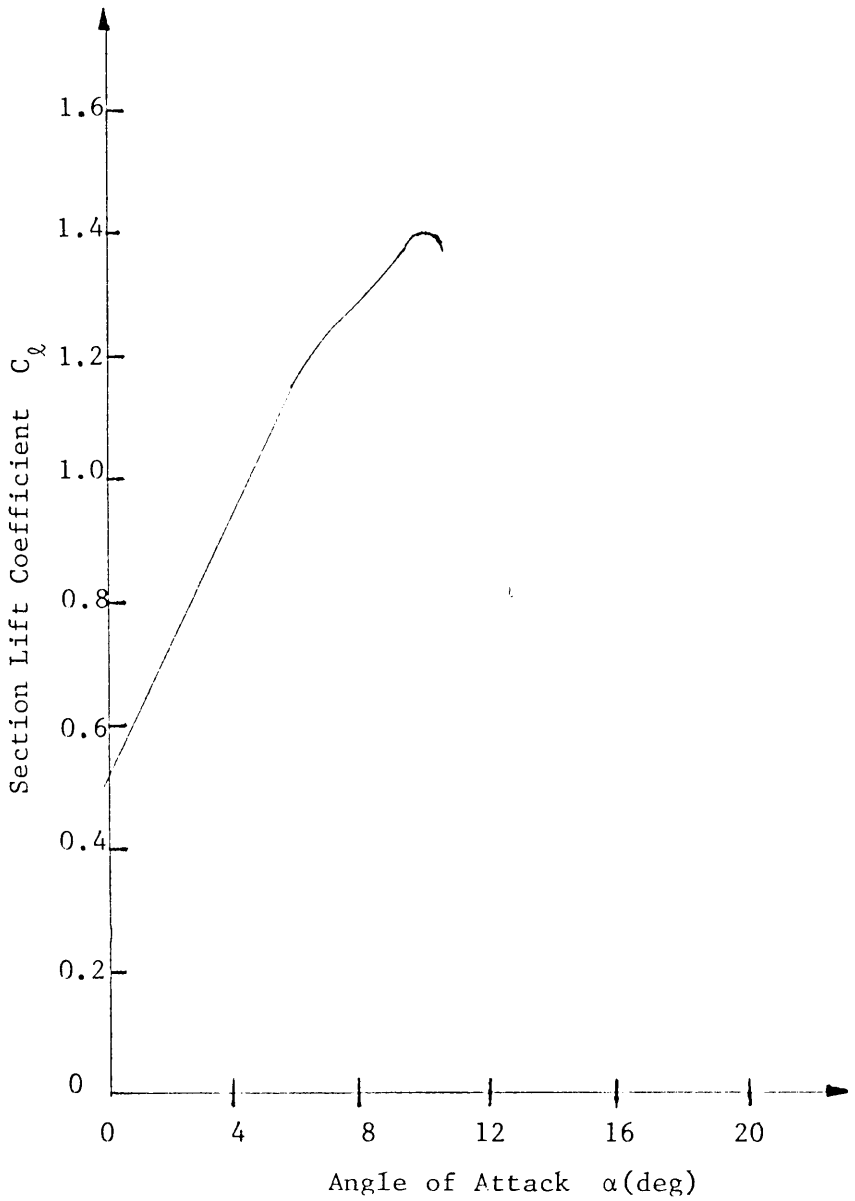

Figure 6. C_ℓ - α Curve for BoAR 80-RPVT-163 Airfoil

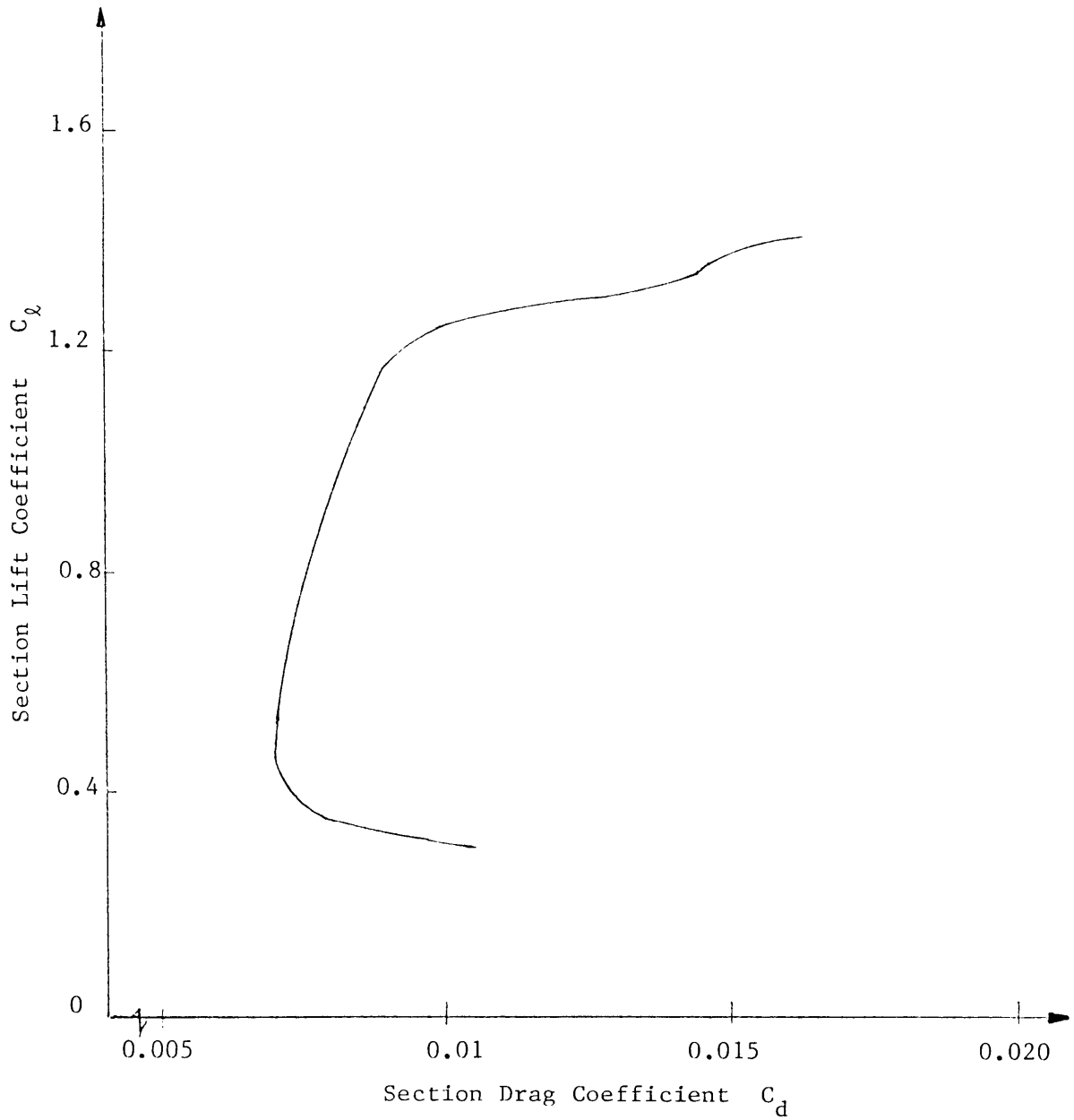

Figure 7. C_ℓ - C_d Curve for BoAR 80-RPVT-163 Airfoil

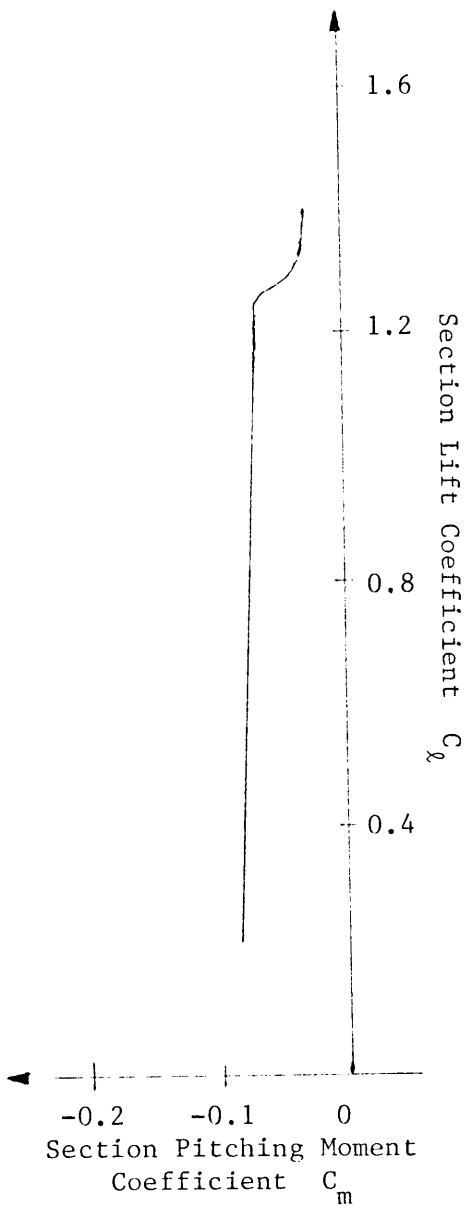

Figure 8. C_ℓ - C_m Curve for BoAR 80-RPVT-163 Airfoil

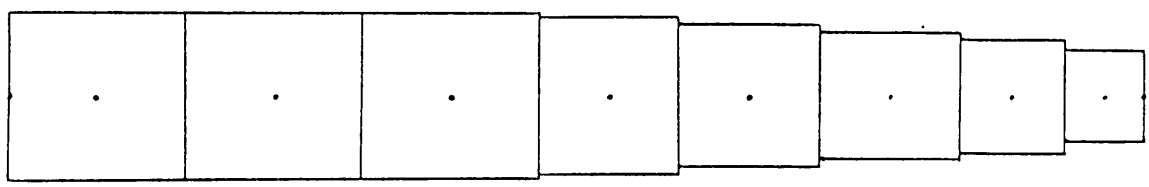

Figure 9. Wing Divided into Constant Cross-Section Elements

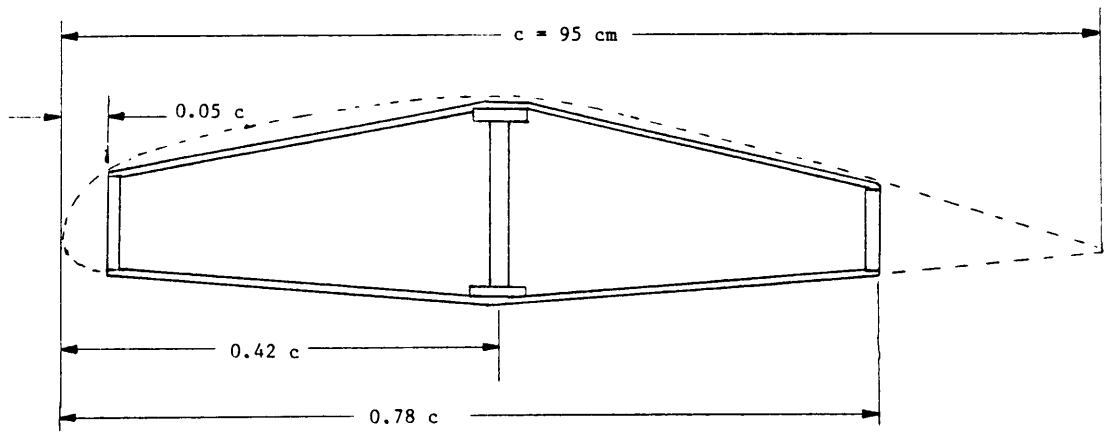

Figure 10. Cross-Section of Wing Element

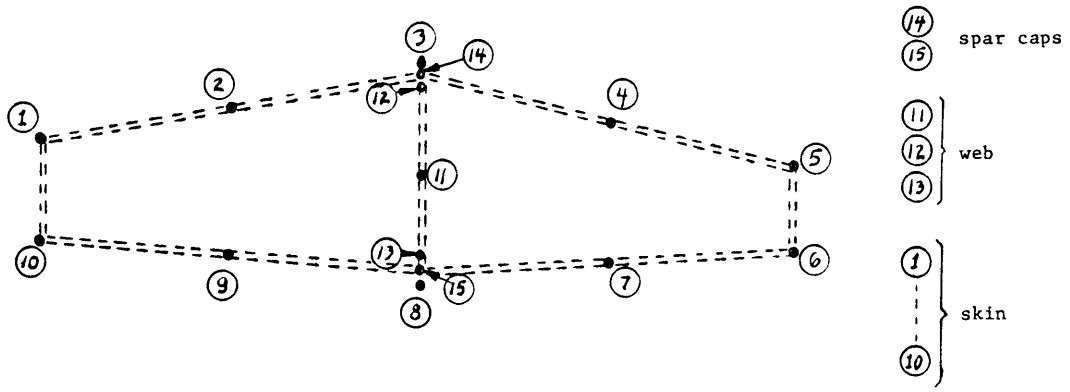

Figure 11. Cross-Section of Wing Element With Stringers

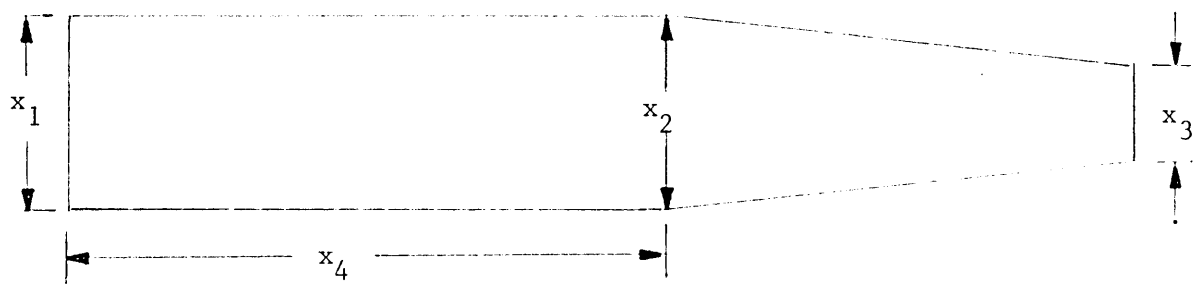

Figure 12. Planform Geometry Variables

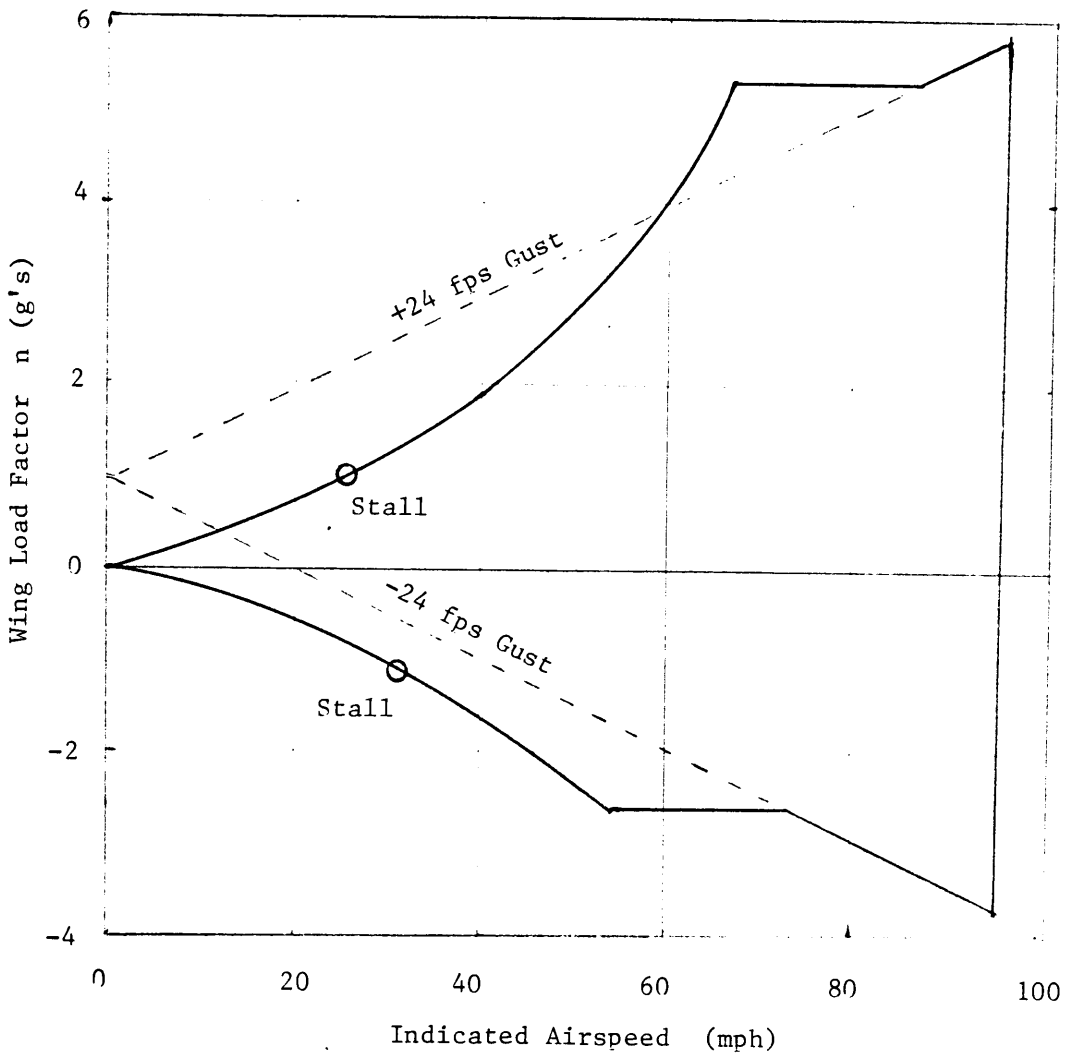

Figure 13. V-n Diagram for the RP-2

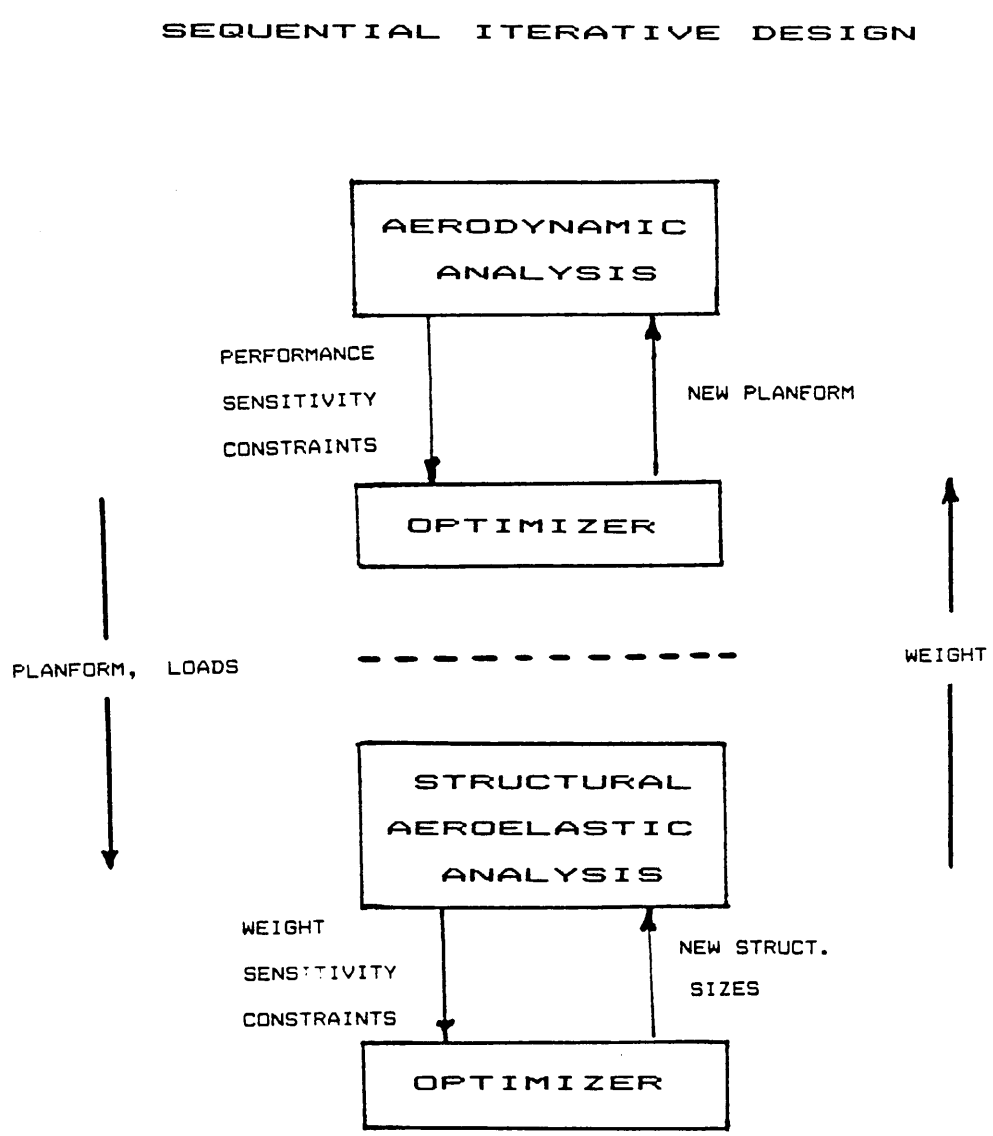

Figure 14. Schematic of Iterative Design Procedure

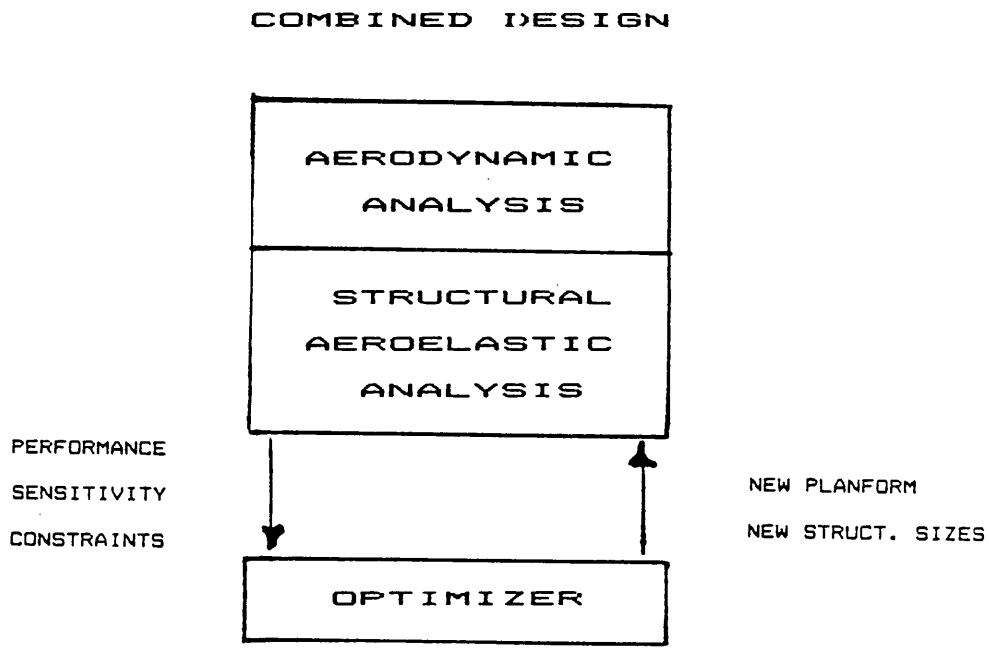

Figure 15. Schematic of Combined Design Procedure

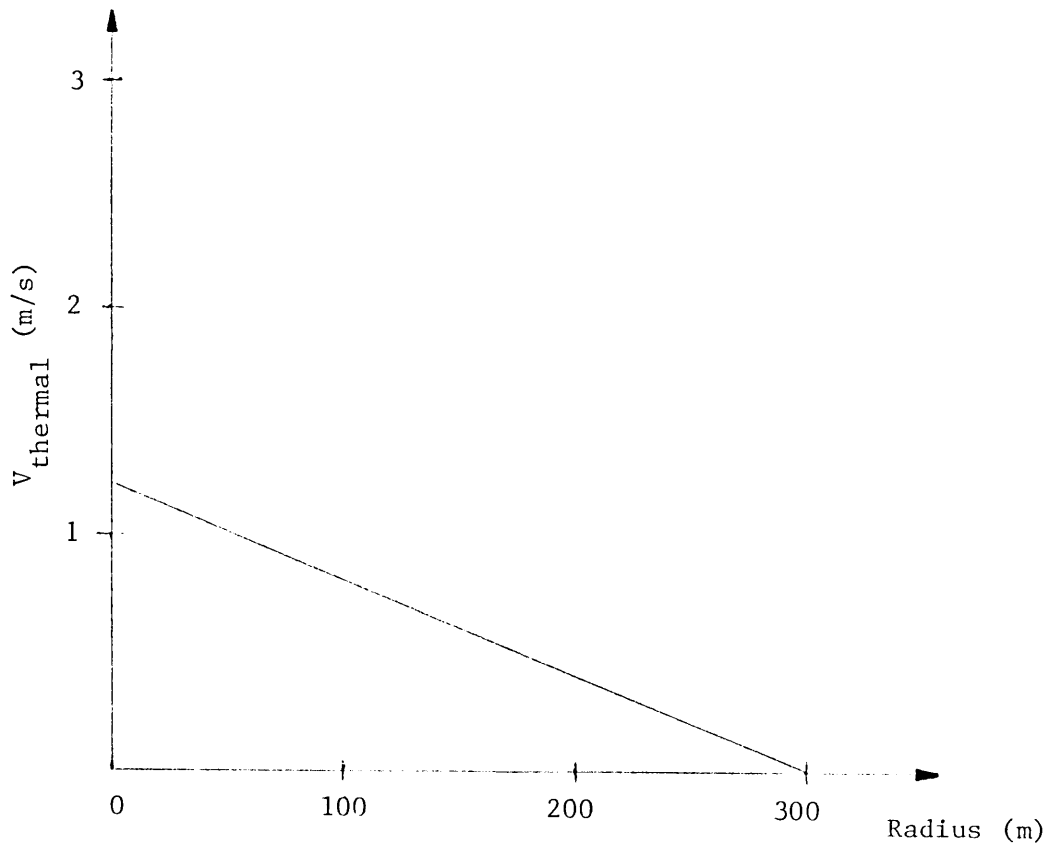

Figure 16. Very Weak Horstmann Thermal

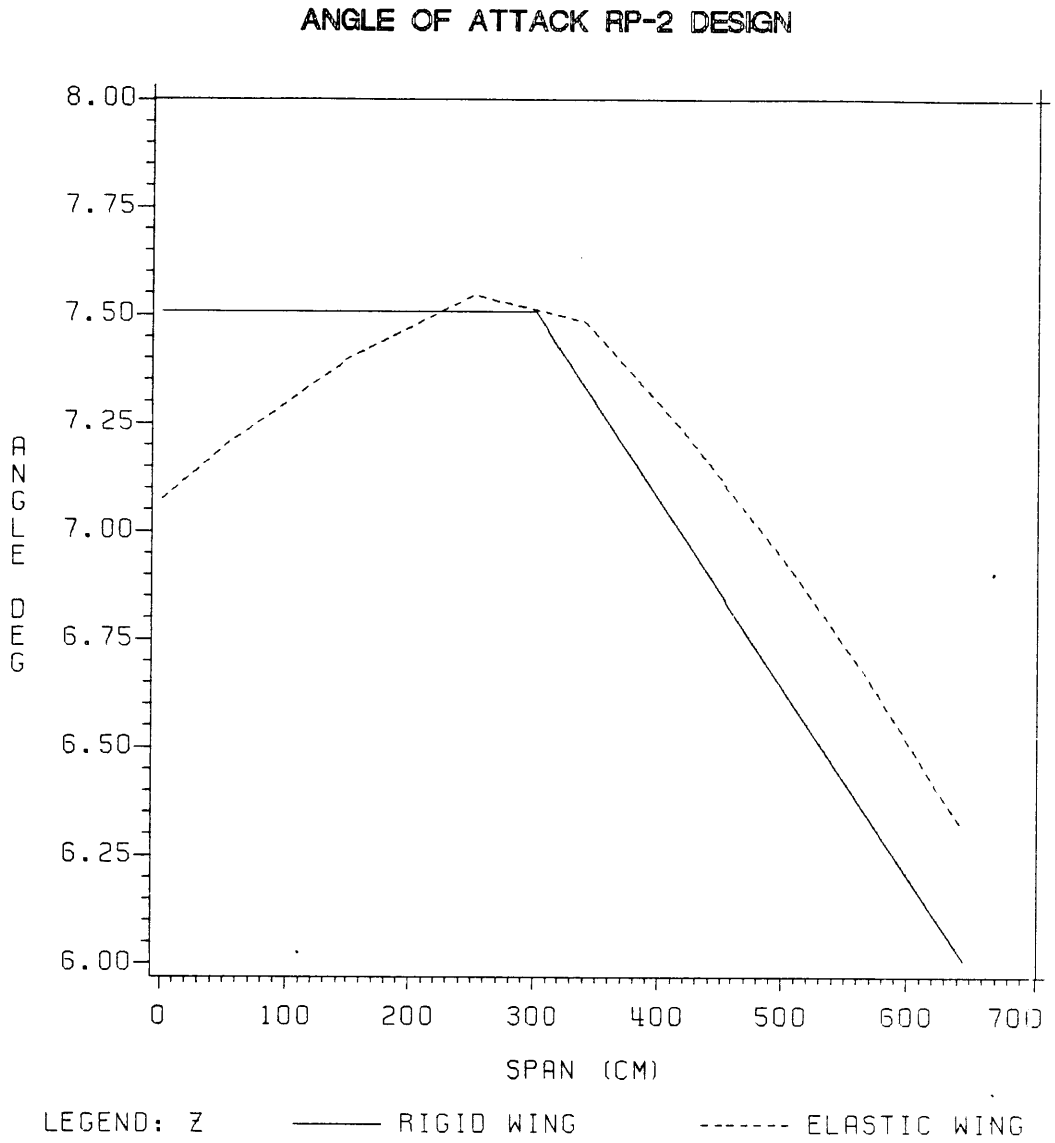

Figure 17. Angle of Attack Distribution for RP-2 Design at 5.9 g

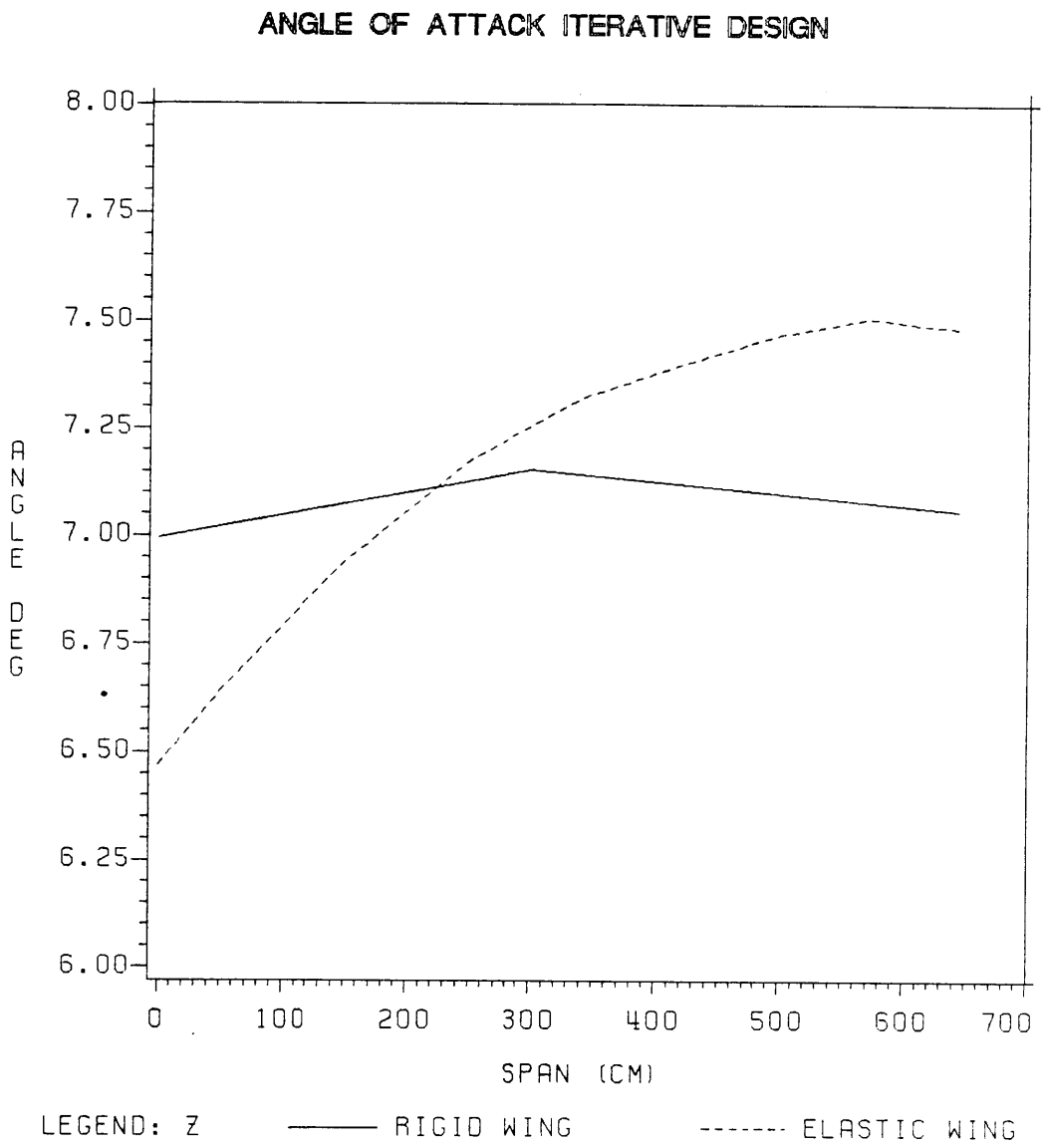

Figure 18. Angle of Attack Distribution for Iterative Design at 5.9 g

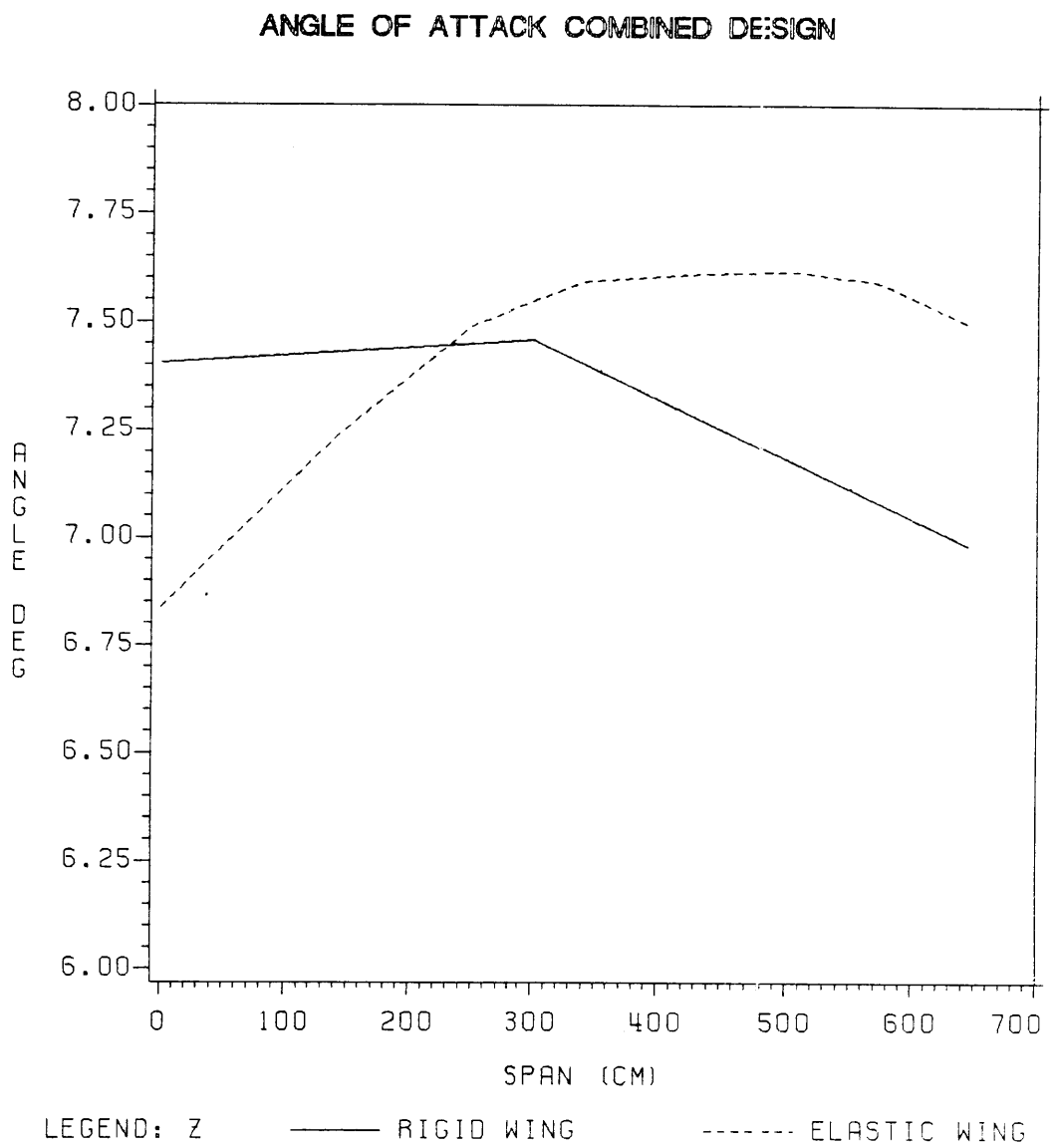

Figure 19. Angle of Attack Distribution for Combined Design at 5.9 g

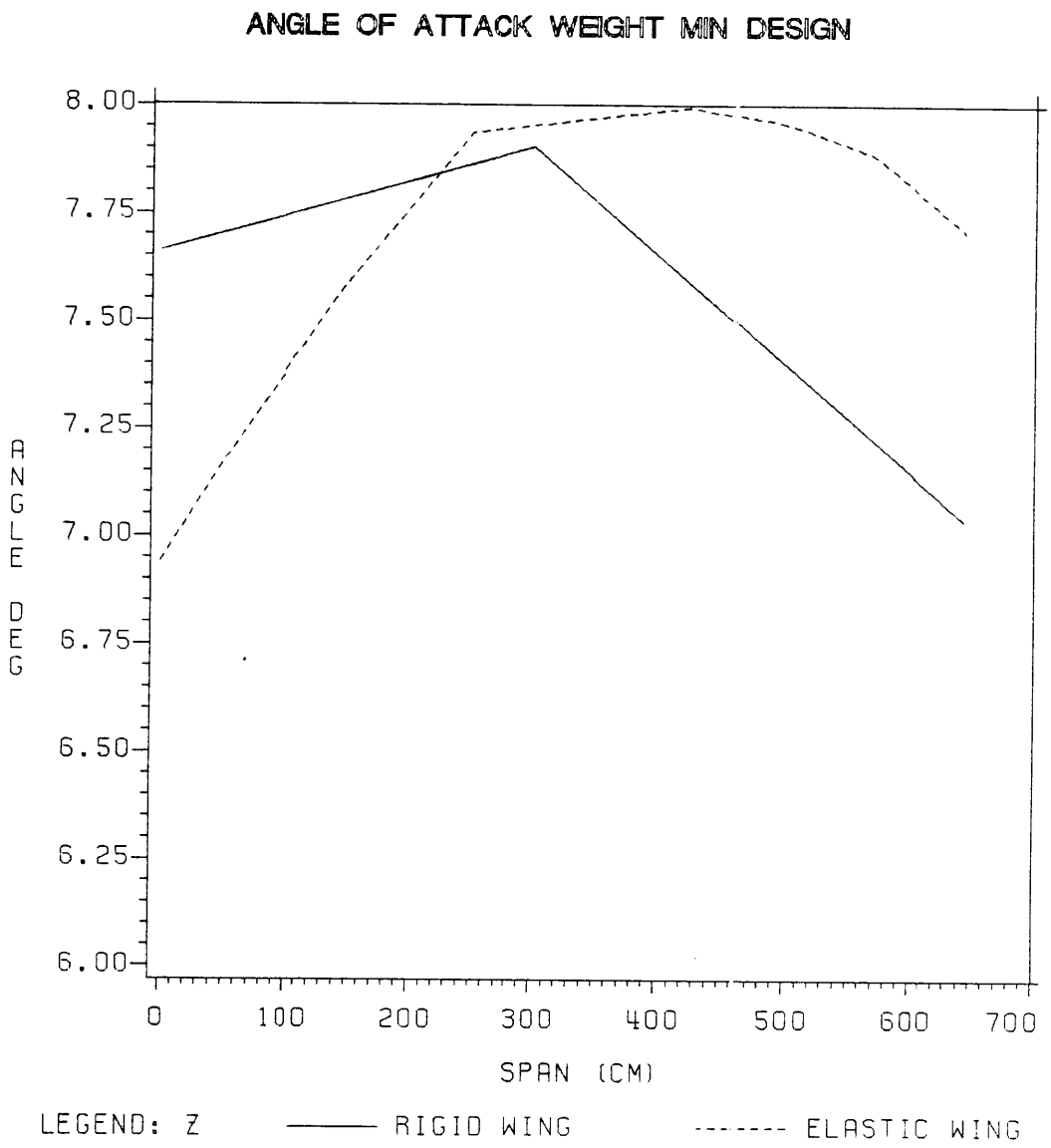

Figure 20. Angle of Attack Distribution for Weight Minimization Design at 5.9 g

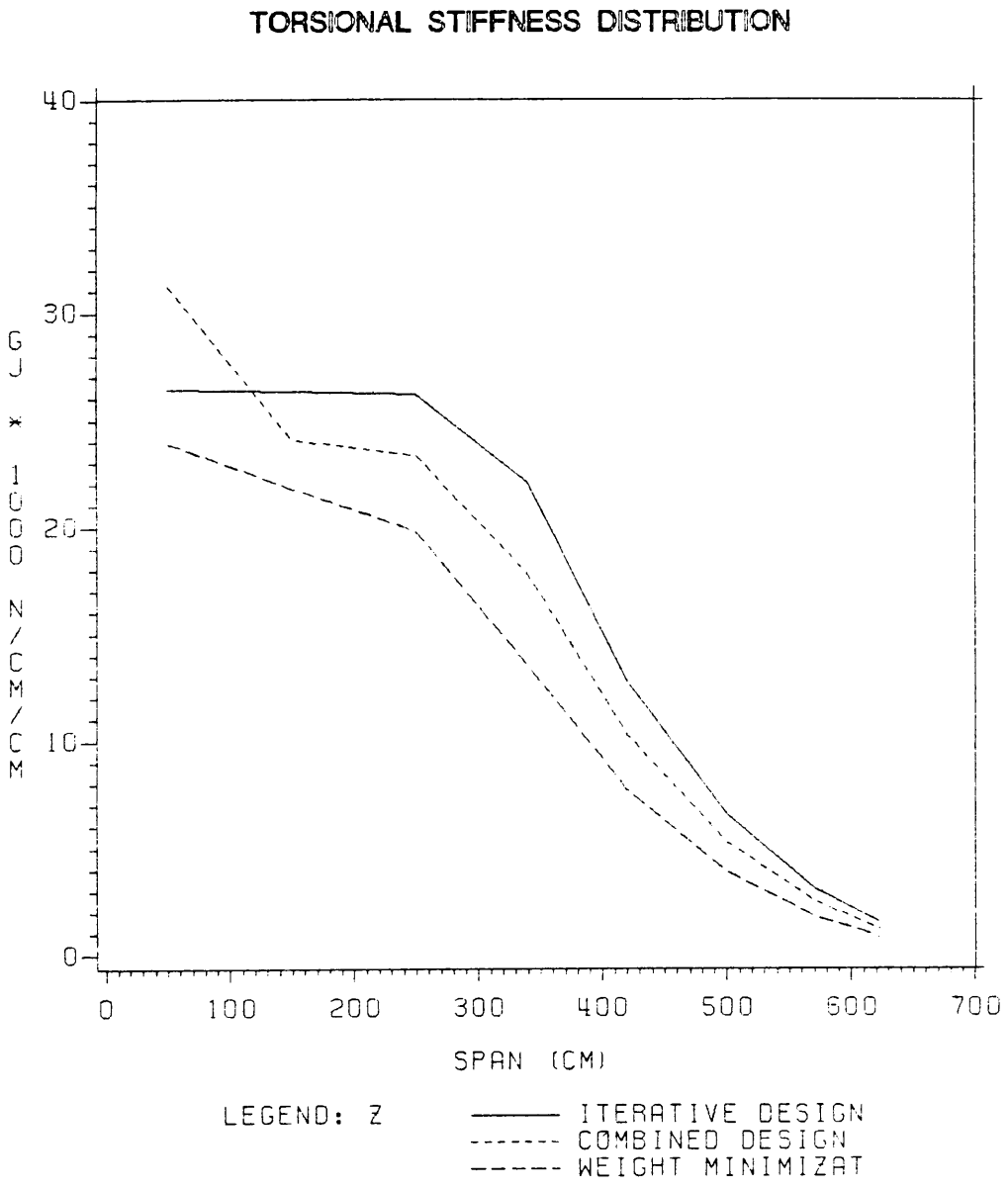

Figure 21. Torsional Stiffness Distribution for 13.5 Meter Designs at 5.9 g

APPENDIX A. SINK SPEEDS FOR PERFORMANCE CALCULATIONS

A.1 SINK SPEED DURING SPIRALLING FLIGHT

For gliding flight in a turn where the flight path has a small downward angle as shown

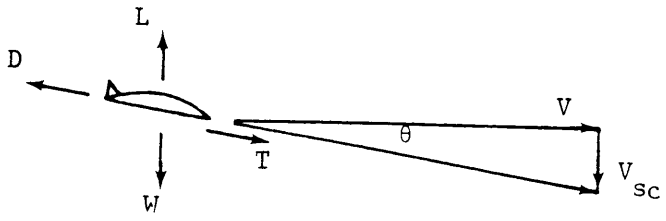

where V_{sc} is the sink speed in the turn, We assume that

$$T = D \quad \text{and} \quad L = nW$$

where n is the load factor and is defined as

$$n = 1/\cos\phi$$

where ϕ is defined as the bank angle as shown

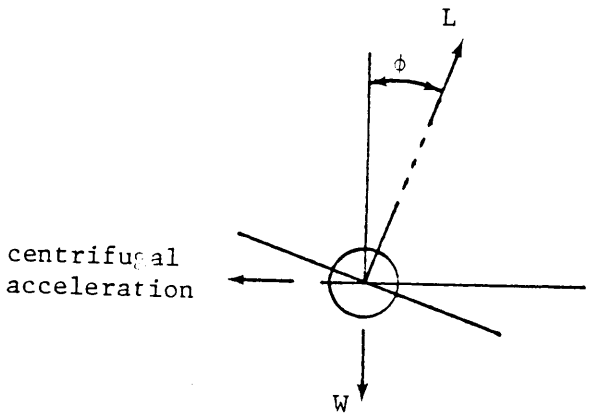

By definition

$$\sin\theta = V_{sc}/v$$

and, because thrust comes only from the weight of the sailplane,

$$T = W \sin\theta$$

and noting again that

$$T = D \quad \text{and} \quad L = nW$$

We obtain

$$nD = L \sin\theta \quad \text{or} \quad \sin\theta = nD/L$$

By definition

$$L = C_L(0.5)\rho V^2 S \quad \text{and} \quad D = C_D(0.5)\ \rho V^2 S$$

where S is the wing planform area. So now we can simplify the equation for sinθ to

$$\sin\theta = nC_D/C_L$$

Substituting into the earlier equation for sinθ we obtain

$$nC_D/C_L = V_{sc}/V$$

Solving for V_{sc}

$$V_{sc} = nVC_D/C_L$$

Noting that

$$L = nW = C_L(0.5)\rho V^2 S$$

and solving for V yields

$$V = \left(\frac{2nW}{\rho S C_L}\right)^{0.5}$$

We can now obtain

$$V_{sc} = \frac{C_D}{C_L^{1.5}} \; n^{1.5} \left(\frac{2W}{\rho S} \right)^{0.5}$$

or

$$V_{sc} = \frac{C_D}{C_L^{1.5}} (\cos\phi)^{1.5} \left(\frac{2W}{\rho S} \right)^{0.5}$$

The expression for cos ϕ must be found. We start by equating horizontal forces in the turn

$$L\sin\phi = WV^2/gR$$

where g is the acceleration due to gravity and R is the radius of the turn. Substituting the expression found for the velocity, V,

$$L\sin\phi = \frac{W}{gR} \frac{2L}{C_L \rho S}$$

and simplifying

$$\sin\phi = \frac{2W}{\rho S C_L g R}$$

Using basic trigonometric functions, it can be shown that

$$\cos\phi = (1 - \sin^2\phi)^{0.5}$$

Substituting in the expression for sinϕ yields

$$\cos\phi = \left[1 - \left(\frac{2W}{\rho S C_L g R}\right)^2\right]^{0.5}$$

And then substituting this into the expression found for V_{sc} results in the final form of the sink speed in the turn as

$$V_{sc} = \frac{C_D}{C_L^{1.5}}\left[1 - \left(\frac{2W}{\rho S C_L g R}\right)^2\right]^{-0.75}\left(\frac{2W}{\rho S}\right)^{0.5}$$

A.2 SINK SPEED DURING CRUISE

For level, gliding flight with a small downward flightpath angle as shown

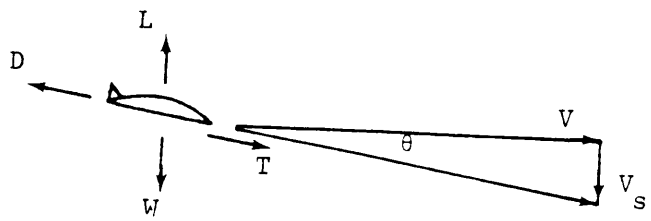

where V_s is the sink speed, by definition

$$\sin\theta = V_s/V$$

Because the thrust comes only from the weight,

$$T = W\sin\theta$$

But, assuming

$$T = D \quad \text{and} \quad L = W$$

we obtain

$$D = L\sin\theta \quad \text{and} \quad \sin\theta = D/L$$

By definition

$$L = C_L(0.5)\rho V^2 S \quad \text{and} \quad D = C_D(0.5)\ \rho V^2 S$$

so we now have

$$\sin\theta = C_D/C_L$$

Substituting into the earlier equation for $\sin\theta$, we obtain

$$C_D/C_L = V_s/V$$

Solving for V_s yields

$$V_s = C_D V / C_L$$

And solving for velocity from the equation

$$L = W = C_L (0.5) \rho V^2 S$$

yields

$$V = \left(\frac{2W}{\rho S C_L} \right)^{0.5}$$

We obtain the final result for the sink speed as

$$V_s = \frac{C_D}{C_L^{1.5}} \left(\frac{2W}{\rho S} \right)^{0.5}$$

The vita has been removed from the scanned document